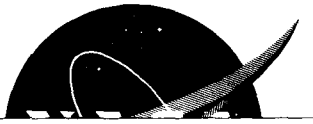

TECHNICAL MEMORANDUM

X-765

SUMMARY OF AERODYNAMIC CHARACTERISTICS OF A WINGED REENTRY VEHICLE AT MACH NUMBERS FROM 0.06 TO 9.6 WITH DETAILED RESULTS AT A MACH NUMBER OF 9.6

By Charles L. Ladson

Langley Research Center
Langley Station, Hampton, Va.

NATIONAL AERONAUTICS AND SPACE ADMINISTRATION
WASHINGTON

March 1963

NATIONAL AERONAUTICS AND SPACE ADMINISTRATION

TECHNICAL MEMORANDUM X-765

SUMMARY OF AERODYNAMIC CHARACTERISTICS OF A WINGED REENTRY VEHICLE AT MACH NUMBERS FROM 0.06 TO 9.6 WITH DETAILED RESULTS AT A MACH NUMBER OF 9.6*

By Charles L. Ladson

SUMMARY

Tests have been conducted at the National Aeronautics and Space Administration, Langley Research Center to determine the effects of Mach number on some of the more important longitudinal, directional, and lateral stability and control parameters of a winged reentry vehicle. Detailed results obtained at a Mach number of 9.6 and an analysis of these results are presented, as well as a summary of data obtained at subsonic and supersonic speeds.

The results at hypersonic speeds and at angles of attack up to 25°, indicate that increasing the nose-deflection angle from 0° to 10° has a small effect on elevon effectiveness, gives a more positive pitching moment with a slight decrease in longitudinal stability, and increases the directional stability. Changing either the wing airfoil section or the nose cross section has little effect on the aerodynamic characteristics.

A summary of the effects of Mach number on the vehicle characteristics indicates that the maximum lift-drag ratio decreases from a value of 4.4 at subsonic speeds to about half of that value at hypersonic speeds for 0° elevon deflection. Although at subsonic and hypersonic speed the model can trim at angles of attack for maximum lift-drag ratio, a trim problem exists in the supersonic region, and auxiliary trim devices may be necessary. In general, both elevon and rudder effectiveness decrease with increasing Mach number. Use of differential elevon deflection to produce a rolling moment is accompanied by an adverse yawing moment throughout the Mach number range. The vehicle is directionally stable except at low angles of attack in the higher Mach number range. In this case, the vehicle can be stabilized by deflecting both rudders outboard with little penalty in longitudinal performance.

/

*Title, Unclassified.

INTRODUCTION

Considerable data have been published on the static aerodynamic characteristics of winged reentry vehicles throughout the Mach number range in recent years. Some of the effects of Mach number on maximum lift-drag ratio and longitudinal and directional stability characteristics have been summarized. (See refs. 1, 2, and 3, for example.) A program has been undertaken at the NASA Langley Research Center to investigate the effects of Mach number variation on the aerodynamic characteristics of a winged reentry configuration that is envisioned to operate at angles of attack from that for maximum lift-drag ratio to that for maximum lift. Several configuration variables have also been investigated.

Subsonic and supersonic tests of this configuration have been conducted and the results have been published in references 4 and 5. The tests at hypersonic speeds were conducted at a Mach number of 9.6 at angles of attack up to 25°. The test Reynolds number was about 0.1×10^6 per inch. Since the maximum angle of attack obtained during the tests was limited to 25° as a result of tunnel blockage and strut mechanism considerations, no data at angles of attack near that for maximum lift are available at hypersonic speeds. The effects of nose shape and nose-deflection angle, wing section, and elevon planform geometry were included in the investigation at a Mach number of 9.6.

The purpose of this paper is to present the results obtained at a Mach number of 9.6 with a brief analysis and to summarize some of the more important longitudinal and directional stability and control parameters of this vehicle as a function of Mach number. Data taken from references 4 and 5 as well as from the present tests are included in the summary for angles of attack up to about 25°.

SYMBOLS

b span, in.

C_D drag coefficient, $\frac{\text{Drag}}{qS}$

C_L lift coefficient, $\frac{\text{Lift}}{qS}$

C_l rolling-moment coefficient, $\frac{\text{Rolling moment}}{qSb}$

C_m pitching-moment coefficient about moment center at $0.70c_r$, $\frac{\text{Pitching moment}}{qSc_r}$

C_n yawing-moment coefficient about moment center at $0.70c_r$, $\frac{\text{Yawing moment}}{qSb}$

C_N normal-force coefficient, $\frac{\text{Normal force}}{qS}$

C_Y side-force coefficient, $\frac{\text{Side force}}{qS}$

C_{l_β} rate of change of rolling-moment coefficient with angle of sideslip at zero sideslip angle, $\left(\frac{\partial C_l}{\partial \beta}\right)_{\beta=0^\circ}$, per deg

C_{n_β} rate of change of yawing-moment coefficient with angle of sideslip at zero sideslip angle, $\left(\frac{\partial C_n}{\partial \beta}\right)_{\beta=0^\circ}$, per deg

C_{Y_β} rate of change of side-force coefficient with angle of sideslip at zero sideslip angle, $\left(\frac{\partial C_Y}{\partial \beta}\right)_{\beta=0^\circ}$, per deg

c_r wing root chord (from theoretical apex to base of body)

L/D lift-drag ratio

M Mach number

q free-stream dynamic pressure, lb/sq in.

S planform area (including area of elevons), sq in.

α angle of attack, deg

β angle of sideslip, deg

δ_a aileron-deflection angle $\left(\delta_{e,R} - \delta_{e,L}\right)$

δ_e elevon-deflection angle (positive for trailing edge down), deg

δ_n nose-deflection angle (positive for nose up), deg

δ_r rudder-deflection angle (positive for trailing edge left), deg

Δ incremental value

Subscripts:

max	maximum
L	left
R	right

Model component designations:

B	body
E_1	elevon, large, full span, hinge line at wing trailing edge
E_2	elevon, outboard mounted, hinge line at wing trailing edge
E_3	elevon, outboard mounted, hinge line 0.712 inch ahead of wing trailing edge
E_4	elevon, small, full span, hinge line at wing trailing edge
F	vertical fin, wing tip mounted
W_1	wing, flat-plate section
W_2	wing, half-diamond section with leading-edge angle of 12°
W_3	wing, half-diamond section with leading-edge angle of 6.5°

MODELS AND DESIGNATIONS

Three-view drawings showing details of the model, vertical fin, various elevons, and nose modifications are presented in figure 1.

The model was constructed of stainless steel and had interchangeable wings, noses, tails, and elevons. The lower surface of the wing was flat, and the nose incidence could be set at 0°, 5°, or 10°. In changing the nose incidence, the nose radius and model length were held constant, and the ridge line of the nose was faired into the body at station 3.280. Tip-mounted vertical fins with rudders were incorporated to provide directional stability and control. The rudders were 60 percent of the fin area and could be deflected outward from 0° to 25°. Trailing-edge elevons were used for longitudinal control and could be deflected from 10° to -30°. The elevons were formed by continuing the upper and lower surfaces of the wing as shown in the section view in figure 1(a) and had a constant trailing-edge thickness. The E_1 and E_2 elevons (fig. 1(b)) have about the same area moment (product of elevon area and distance from elevon centroid of area to model center of gravity) and would thus be expected to have about the

same effectiveness. A photograph of configuration BW_2E_2F is shown in figure 2(a), and a photograph of the various model components is shown in figure 2(b).

All coefficients are based on wing planform area (which includes elevons), span, and wing root chord. The values of these reference areas and lengths are presented in table I. The moment center for the data is at $0.70c_r$ and $0.0605c_r$ above the lower surface of the wing.

APPARATUS, TESTS, AND PROCEDURE

The data contained herein were obtained in the Langley 11-inch hypersonic tunnel at Mach numbers of 6.8 and 9.6 with most of the data being at the higher Mach number. At $M = 9.6$, the stagnation pressure was about 42 atmospheres, the stagnation temperature was 1,100° F, and the Reynolds number was about 0.1×10^6 per inch. At $M = 6.8$, the stagnation pressure was about 20 atmospheres, the stagnation temperature was 650° F, and the Reynolds number per inch was about 0.2×10^6. Calibrations for the two tunnel nozzles are presented in references 6 and 7.

All tests were made with the use of a six-component water-cooled strain-gage balance. The angles of attack of the model were measured optically by use of a light beam reflected from a prism mounted flush with the surface of the model onto a calibrated scale. This method gave the true angle of attack of the model, including the deflection of the model and sting under load. Base-pressure measurements were made at both Mach numbers, and the axial-force data have been corrected to correspond to a base pressure equal to the free-stream static pressure. At $M = 9.6$, these corrections are negligible in comparison with the measured axial force.

All longitudinal data were obtained for angles of attack from -5° to 25°. The directional and lateral stability data were obtained from tests at sideslip angles of 0°, 2°, and 4° and angles of attack up to 25°.

RESULTS OF TESTS AT HYPERSONIC SPEEDS

The results from the tests at hypersonic speeds are presented in figures 3 to 15. An index to the various plots is presented in table II. All longitudinal performance data are referred to the stability axis system, while the directional, lateral, and longitudinal stability results are referred to the body axis.

Longitudinal Characteristics

The longitudinal aerodynamic characteristics of the configuration with elevons E_1 and E_2 are presented in figures 3, 4, and 5 for nose-deflection angles of 0°, 5°, and 10°. From these data it is seen that increasing the nose incidence at a constant angle of attack gives a substantial positive increment in

pitching moment as would be expected, and also reduces the longitudinal stability. This loss of stability is a result of the increased rate of change of loading on the nose which is well ahead of the vehicle center of gravity. It should also be noted that to maintain trim at a given angle of attack, increasing nose deflection must also be accompanied by a positive elevon deflection which in turn increases the vehicle stability. Thus, for a trimmed condition at a constant angle of attack, increasing nose deflection will result in increased vehicle stability. At angles of attack near that for maximum lift, the anticipated effect of nose deflection would be to increase the vehicle stability (ref. 3). The effect of nose deflection is also evident on the incremental pitching moment obtained at various elevon-deflection angles. Comparing figures 3(d) and 5(d), it can be seen that increasing δ_n from 0° to 10° decreases the elevon effectiveness for positive angles of attack and positive elevon deflections and increases the elevon effectiveness for negative angles of attack and negative elevon-deflection angles. Thus, the more nearly the nose is alined with the flow, the higher the elevon effectiveness is seen to be when the elevon is deflected into the flow. This is due to the increased losses across the shock wave as the deflection angle between the nose and the wind increases. Little effect of nose deflection on the maximum lift-drag ratio of the configuration is observed.

In figure 6, the E_2 and E_3 elevon characteristics are compared for the configuration with the flat-plate, W_1 wing. The point to be noted is that by moving the elevon hinge line forward on the vehicle, the lifting area behind the vehicle center of gravity is reduced and the stability of the configuration decreases.

The characteristics of the E_4 elevon are presented in figure 7. Since this elevon has one-half the chord of the E_1 elevon, the incremental pitching moment should be about one-half that for the E_1 elevon. Comparison of figures 4(c) and 7(b) shows that this is the case and thus elevon effectiveness for this type of elevon is a nearly linear function of elevon area.

For all elevons tested (figs. 3 to 7), a positive elevon deflection resulted in an increase in stability and a negative deflection resulted in a decrease in longitudinal stability. This has also been noted on tests of similar models in references 8 and 9. Elevon deflection also has little effect (less than 0.3) on the value of the maximum lift-drag ratio at hypersonic speeds because of the low lift-drag ratio of the configuration but does affect the angle of attack for maximum L/D.

The effect of the vertical fins on the longitudinal stability is seen in figure 8(b). The positive increment in pitching moment which results from addition of the fins is a result of the normal and axial force of the fins as well as a high-pressure region on the wing upper surface due to the fin shock. These effects are reduced as angle of attack is increased and are reflected in the data.

Few effects of changes in either wing section or modification to the nose section are noted in the data presented in figure 9. The modification to the nose section was made in an effort to eliminate the longitudinal instability of the vehicle which exists at low angles of attack (see fig. 4(d)). Other modifications to nose shape on a similar vehicle were investigated and the results in

reference 10 show that very large modifications to the nose geometry have little effect on this low-angle-of-attack instability problem. Reference 10 does show that this instability can be reduced by use of a body flap located on the upper surface at the rear of the body.

Data on the configuration with elevon E_1 at a Mach number of 6.8 are presented in figure 10. Comparison of data at $M = 6.8$ and at $M = 9.6$ is presented under the section entitled "Summary of Mach Number Effects."

Directional and Lateral Control

The yaw control characteristics are shown in figure 11(a). At the higher rudder-deflection angles of the tests, yaw control decreases rather sharply with increasing angle of attack for angles of attack above about 12°. This is a result of the low effective flow-deflection angle between the rudder and the wind caused by the swept rudder hinge line. A small adverse rolling moment due to yaw control exists for all angles of attack because the center of pressure of the rudder is above the vehicle center of gravity. Increasing the rudder deflection angle increases the drag of the vehicle, and in turn reduces the maximum lift-drag ratio slightly (fig. 11(b)) for the maximum deflection angle of the tests. Little effect of rudder deflection on pitching moment is noted in figure 11(c).

Roll control characteristics due to differential deflection of the E_2 elevons are presented in figure 12(a). The control effectiveness increases rather rapidly with increasing angle of attack as is expected since the flow-deflection angles of the elevons are increasing. A large adverse yawing moment results from the differential elevon deflection. This yaw is due to the differential axial-force components of the down elevons. The vehicle was also tested with the vertical fins removed and, as seen in figure 12(a), the fins had essentially no effect on either rolling moment or yawing moment. Differential elevon deflection slightly decreases the maximum lift-drag ratio (fig. 12(b)), and both lift and drag are increased. This differential elevon deflection has a large effect on the pitching moment as seen in figure 12(c), even though the average elevon deflection angle was held at 0° for the data shown.

Directional and Lateral Stability

The effects of nose-deflection angle on the directional and lateral stability characteristics are shown in figure 13. Increasing the nose-deflection angle increases the directional stability at angles of attack up to 20° as a result of shielding the upper portion of the nose of the vehicle from the flow, thus reducing its destabilizing effect. At low angles of attack, positive values of C_{l_β} exist as noted previously on this type of configuration (see refs. 8 and 11). With the nose deflected upward, the side-force component of the nose input is raised relative to the body axis and contributes to the negative increment in C_{l_β} as a result of the nose deflection shown in figure 13.

As noted in figure 13, the basic configuration does not have positive directional stability at angles of attack below about 12°. To provide stability in this angle-of-attack range, both rudders can be deflected outward as seen in figure 14(a). This positive increment in stability is a result of the increased effectiveness of the vertical surfaces due to their increased flow-deflection angle. These trends have been noted previously in reference 8. Deflecting both rudders outboard decreases the maximum lift-drag ratio slightly but has little effect on the pitch characteristics as seen in figures 14(b) and 14(c).

As seen in figure 15, changes in wing airfoil section have an effect on C_{Y_β} as expected, but, due to the small lever arm through which the side force acts, have little effect on the directional stability parameter C_{n_β} or the lateral stability parameter C_{l_β}.

SUMMARY OF MACH NUMBER EFFECTS

Summary plots of the effects of Mach number on some of the more important aerodynamic characteristics of the configuration are presented in figures 16 through 21. The data at subsonic speeds (M = 0.06) are from reference 4 while data at supersonic speeds (M = 1.50, M = 2.96, and M = 4.63) are from reference 5.

Longitudinal Characteristics

Data in reference 5 indicate the configuration does not have stable trim points at low angles of attack $\left(\text{near } (L/D)_{max}\right)$, and thus the summary plots presented are for constant elevon deflection or constant angle of attack rather than for trimmed conditions. The maximum lift-drag ratio and angle of attack at which it occurs are plotted as a function of Mach number for elevon deflection angles of 0° and -10° in figure 16. These elevon-deflection angles are in the range of that required for trim at subsonic and hypersonic speeds. At subsonic speeds, the lift-drag ratio is about 4.4 for 0° elevon deflection and drops to about half this value at hypersonic speeds. These values and the trend with Mach number are similar to the results obtained on configurations of the same type in references 1 and 10. The angle of attack for maximum lift-drag ratio increases as the elevon-deflection angle decreases from 0° to -10° at subsonic speeds, while little effect is noted at hypersonic speeds. The reason for this can be seen from noting that at subsonic speeds (ref. 4), a negative elevon deflection displaces both the lift and drag curves (and the lift-drag ratio) in a positive angle-of-attack direction. At hypersonic speeds, only the lift-curve slope changes so that the maximum lift-drag ratio occurs at about the same angle of attack.

The longitudinal stability and trim characteristics are presented in figure 17 as plots of pitching moment against angle of attack for the various Mach numbers and for elevon-deflection angles of 0°, -10°, and 10°. These deflection angles were chosen since test results are available throughout the Mach number

range. With $\delta_e = 0^\circ$, the configuration is stable and trimmed at hypersonic speeds at an angle of attack slightly above that for maximum lift-drag ratio ($\alpha \approx 16^\circ$). As the Mach number decreases, the pitching-moment coefficient becomes more negative and at Mach number of 4.63 and below, no stable trim point exists for $\delta_e = 0^\circ$. With an elevon deflection angle of -10° (fig. 17(b)), unstable trim points are obtained at the supersonic speeds. Thus, as stated in reference 5, to trim at angles of attack near $(L/D)_{max}$ at supersonic speeds, a corrective device which would increase both the pitching moment at zero lift and the stability level is required. At $M = 0.06$ and $M = 1.50$, pitch-up occurs at angles of attack of about 15° to 20°, depending upon elevon-deflection angle. Stable trim can be obtained at angles of attack up to those for pitch-up at these two Mach numbers. At subsonic speeds, elevon-deflection angles between 0° and -10° would be required for trim, but at $M = 1.50$, elevon-deflection angles of more than -10° would be required to trim at angles of attack up to that for pitch-up.

As seen in figure 18, the elevon effectiveness decreases with increasing Mach number as is expected, and the nonlinearity of the curves tends to increase with increasing Mach number. It should also be noted that at 0° angle of attack, the elevon effectiveness is very low at $M = 9.6$, but increases as the angle of attack increases. This low effectiveness at low angles of attack is characteristic of this type of configuration. (See refs. 8 and 9.)

Directional and Lateral Control

The directional control characteristics of the configuration are presented in figure 19 for angles of attack of 0° and 25°. For tests at $M = 2.96$ and $M = 4.63$, the hinge line of the rudder was vertical, not swept as for the subsonic and hypersonic speeds, and the rudder was also slightly smaller. In general, rudder effectiveness decreases with increasing Mach number and also decreases rapidly with increasing angle of attack. The decrease in rudder effectiveness with increasing angle of attack is expected since the flow-deflection angle of the rudder with respect to the wind decreases with increasing angle of attack. An adverse rolling moment due to rudder deflection is also noted at all Mach numbers since the center of pressure of the rudder (assumed to be near the centroid of area) is above the model center of gravity. At $\alpha = 0^\circ$, Mach number has little effect on the magnitude of the adverse rolling moment.

The lateral control characteristics of the configuration are presented in figure 20 for angles of attack of 0° and 25°. As seen in this figure, roll effectiveness also generally decreases with increasing Mach number but increases with increasing angle of attack as is expected since the deflection angle between the down elevon and the wind increases. A large adverse yawing moment is noted at all Mach numbers for the differentially deflected elevons. At subsonic speeds (ref. 4), this adverse yawing moment is attributed to induced loads on the inner surface of the vertical fin produced by the differential deflection of the elevons. As mentioned under "Results of Tests at Hypersonic Speeds," the vertical tails had essentially no effect on the adverse yawing moment at hypersonic speeds. In this speed regime, the yaw is a result of the axial force on the down elevon being greater than that on the up elevon, thus creating a yaw due to the differential axial force. This same trend has been noted previously on a similar model

(ref. 8). Attempts to alleviate this adverse yaw at hypersonic speeds have been made by sweeping the elevon hinge line forward so that the line of action of the axial force is through the model center of gravity. Results of this modification to a $L/D = 0.5$ lifting-body configuration in reference 12 show that by use of hinge-line sweep this adverse yaw can be eliminated.

Directional and Lateral Stability Characteristics

Directional and lateral stability characteristics are shown in figure 21 plotted against angle of attack. Except for the subsonic-speed regime, the directional stability parameter C_{n_β} decreased with increasing Mach number and, at the two higher Mach numbers, a region of instability exists at the lower angles of attack. This instability at low angles of attack can be overcome at hypersonic speeds by deflecting both rudders outward as was shown in the previous section entitled "Results of Tests at Hypersonic Speeds." The increase in directional stability with increasing angle of attack, as mentioned previously, is attributed to the shielding of the nose, thus decreasing its destabilizing effect.

Little effect of Mach number in the supersonic and hypersonic range is noted on the lateral stability parameter C_{l_β}. As has been noted on similar models in the past (refs. 8 and 9), a positive C_{l_β} exists at angles of attack below about 8° probably because of body-wing interference effects. At subsonic speeds, a much larger negative C_{l_β} is noted.

CONCLUDING REMARKS

Tests have been conducted at the NASA, Langley Research Center to determine the aerodynamic characteristics of a winged reentry vehicle at Mach numbers from subsonic to hypersonic. Detailed results at a Mach number of 9.6 as well as a summary of Mach number effects have been presented in this paper.

The results at hypersonic speeds at angles of attack up to 25° indicate that increasing the nose-deflection angle from 0° to 10° has a small effect on elevon effectiveness, gives a more positive pitching moment with a slight decrease in longitudinal stability, and increases the directional stability. Changing either the wing airfoil section or the nose cross section had little effect on the aerodynamic characteristics.

A summary of the effects of Mach number on the vehicle characteristics indicates that the maximum lift-drag ratio decreases from a value of 4.4 at subsonic to about half of that value at hypersonic speeds for a 0° elevon deflection. Although the model can trim at angles of attack for maximum lift-drag ratio at subsonic and hypersonic speeds, a trim problem exists in the supersonic region and auxiliary trim devices may be necessary. In general, both elevon and rudder effectiveness decrease with increasing Mach number. Use of differential elevon deflection to produce a rolling moment is accompanied by a large adverse yawing moment throughout the Mach number range. The vehicle is directionally stable

except at low angles of attack in the higher Mach number range. In this case, the vehicle can be stabilized by deflecting both rudders outboard with little penalty in longitudinal performance.

Langley Research Center,
National Aeronautics and Space Administration,
Langley Station, Hampton, Va., November 23, 1962.

REFERENCES

1. McLellan, Charles H., and Ladson, Charles L.: A Summary of the Aerodynamic Performance of Hypersonic Gliders. NASA TM X-237, 1960.

2. Rainey, Robert W., Fetterman, David E., Jr., and Smith, Robert: Summary of the Static Stability and Control Results of a Hypersonic Glider Investigation. NASA TM X-277, 1960.

3. Rainey, Robert W., and Close, William H.: Studies of Stability and Control of Winged Reentry Configurations. NASA TM X-327, 1960.

4. Ware, George M., and Shanks, Robert E.: Investigation of the Low-Subsonic Flight Characteristics of a Model of a Reentry Configuration Having a 75° Delta Wing. NASA TM X-684, 1962.

5. Reed, James D., and Shaw, David S.: Static Stability and Control Characteristics of a Proposed Winged Reentry Vehicle at Mach Numbers of 1.50, 2.96, and 4.63. NASA TM X-676, 1962.

6. Bertram, Mitchel H.: Exploratory Investigation of Boundary-Layer Transition on a Hollow Cylinder at a Mach Number of 6.9. NACA Rep. 1313, 1957. (Supersedes NACA TN 3546.)

7. Bertram, Mitchel H.: Boundary-Layer Displacement Effects in Air at Mach Numbers of 6.8 and 9.6. NASA TR R-22, 1959. (Supersedes NACA TN 4133.)

8. Ladson, Charles L., and Johnston, Patrick J.: Aerodynamic Characteristics of Two Winged Reentry Vehicles at Supersonic and Hypersonic Speeds. NASA TM X-346, 1961.

9. Ladson, Charles L., and Johnston, Patrick J.: Aerodynamic Characteristics of a Blunt-Nosed Winged Reentry Vehicle at Supersonic and Hypersonic Speeds. NASA TM X-357, 1961.

10. Ladson, Charles L.: Effects of Several Nose and Vertical-Fin Modifications on the Low-Angle-Of-Attack Static Stability of a Winged Reentry Vehicle at Mach Numbers of 9.6 in Air and 17.8 in Helium. NASA TM X-608, 1961.

11. Ladson, Charles L., Johnston, Patrick J., and Trescot, Charles D., Jr.: Effects of Wing Plan-Form Geometry on the Aerodynamic Characteristics of a Hypersonic Glider at Mach Numbers up to 9.6. NASA TM X-286, 1960.

12. Armstrong, William O.: Aerodynamic Characteristics of a Flat-Bottom Canted-Nose Half-Cone Reentry Configuration at a Mach Number of 6.7. NASA TM X-630, 1962.

TABLE I.- MODEL PHYSICAL CHARACTERISTICS

Basic model without elevons:	
Length (from theoretical vertex), in.	7.468
Span, in.	3.480
Planform area, sq in.	14.658
Elevon area (both elevons), sq in.:	
E_1	3.10
E_2	2.92
E_3	2.94
E_4	1.55
(Elevon area)/(Total planform area) for -	
E_1	0.174
E_2	0.166
E_3	0.174
E_4	0.095
Vertical fin area (each), sq in.	2.18
(Rudder area)/(Vertical fin area)	0.60

TABLE II.- INDEX TO HYPERSONIC DATA PLOTS

Configuration	M	δ_n, deg	δ_e, deg	δ_r, deg	Data plotted	Figure
Longitudinal aerodynamic characteristics						
BW_2E_1F	9.6	0	10, 0, -10	0	C_L, C_D, L/D against α	3(a)
BW_2E_2F	9.6	0	10, 0, -10, -20, -30	0	C_L, C_D, L/D against α	(b)
BW_2E_1F	9.6	0	10, 0, -10	0	C_m against C_N	(c)
BW_2E_2F	9.6	0	10, 0, -10, -20, -30	0	C_m against C_N	(d)
BW_2E_1F	9.6	5	10, 0, -10	0	C_L, C_D, L/D against α	4(a)
BW_2E_2F	9.6	5	10, 0, -10, -20, -30	0	C_L, C_D, L/D against α	(b)
BW_2E_1F	9.6	5	10, 0, -10	0	C_m against C_N	(c)
BW_2E_2F	9.6	5	10, 0, -10, -20, -30	0	C_m against C_N	(d)
BW_2E_1F	9.6	10	10, 0, -10	0	C_L, C_D, L/D against α	5(a)
BW_2E_2F	9.6	10	10, 0, -10, -20, -30	0	C_L, C_D, L/D against α	(b)
BW_2E_1F	9.6	10	10, 0, -10	0	C_m against C_N	(c)
BW_2E_2F	9.6	10	10, 0, -10, -20, -30	0	C_m against C_N	(d)
BW_1E_2F	9.6	5	10, 0, -10, -20, -30	0	C_L, C_D, L/D against α	6(a)
BW_1E_3F	9.6	5	10, 0, -10, -20, -30	0	C_L, C_D, L/D against α	(b)
BW_1E_2F	9.6	5	10, 0, -10, -20, -30	0	C_m against C_N	(c)
BW_1E_3F	9.6	5	10, 0, -10, -20, -30	0	C_m against C_N	(d)
BW_2E_4F	9.6	5	10, 0, -10	0	C_L, C_D, L/D against α	7(a)
BW_2E_4F	9.6	5	10, 0, -10	0	C_m against C_N	(b)
BW_2 BW_2E_2 BW_2E_2F	9.6	5	0	0	C_L, C_D, L/D against α	8(a)
BW_2 BW_2E_2 BW_2E_2F	9.6	5	0	0	C_m against C_N	8(b)
BW_2E_2F Basic nose Modified nose	9.6	5	0	0	C_L, C_D, L/D against α	9(a)
BW_1E_2F BW_2E_2F BW_3E_2F	9.6	5	0	0	C_L, C_D, L/D against α	9(b)
BW_2E_2F Basic nose Modified nose	9.6	5	0	0	C_m against C_N	9(c)
BW_1E_2F BW_2E_2F BW_3E_2F	9.6	5	0	0	C_m against C_N	9(d)
BW_2E_1F	6.8	5	0, 10	0	C_L, C_D, L/D against α	10(a)
BW_2E_1F	6.8	5	0, 10	0	C_m against C_N	(b)

TABLE II.- INDEX TO HYPERSONIC DATA PLOTS - Concluded

Configuration	M	δ_n, deg	δ_e, deg	δ_r, deg	Data plotted	Figure
Directional and lateral control						
BW_2E_2F	9.6	5	0	0, -5, -15, -25	C_l, C_n, C_Y against α	11(a)
	9.6	5	0	0, -5, -15, -25	C_L, C_D, L/D against α	(b)
	9.6	5	0	0, -5, -15, -25	C_m against C_N	(c)
BW_2E_2F	9.6	5	0, ±10, ±20	0	C_l, C_n, C_Y against α	12(a)
	9.6	5	0, ±10, ±20	0	C_L, C_D, L/D against α	(b)
	9.6	5	0, ±10, ±20	0	C_m against C_N	(c)
BW_2E_2F	9.6	0, 5, 10	0	0	C_{l_β}, C_{n_β}, C_{Y_β} against α	13
BW_2E_2F	9.6	5	0	0, ±15	C_{l_β}, C_{n_β}, C_{Y_β} against α	14(a)
	9.6	5	0	0, ±15	C_L, C_D, L/D against α	(b)
	9.6	5	0	0, ±15	C_m against C_N	(c)
BW_1E_2, BW_2E_2, BW_3E_2	9.6	5	0	0	C_{l_β}, C_{n_β}, C_{Y_β} against α	15

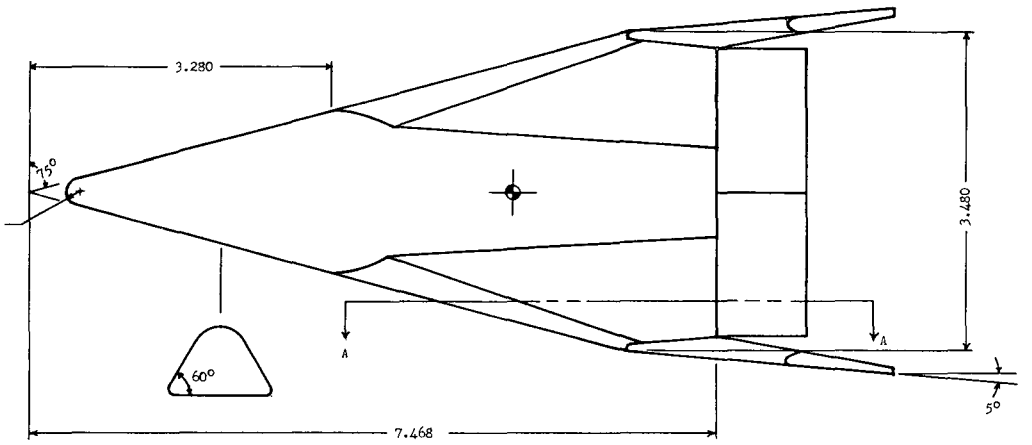

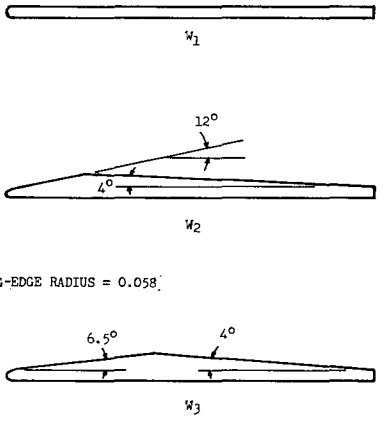

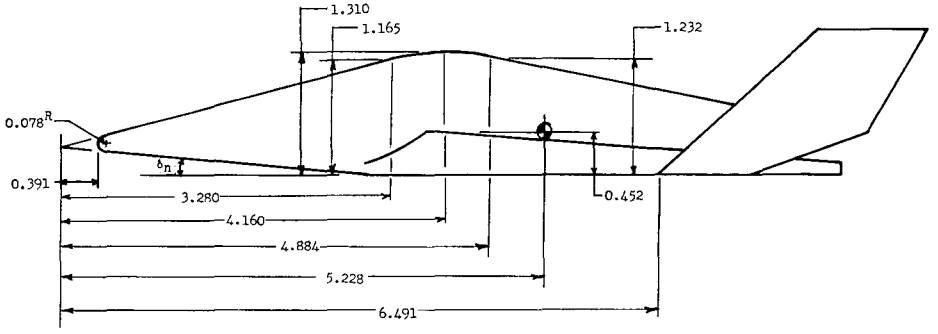

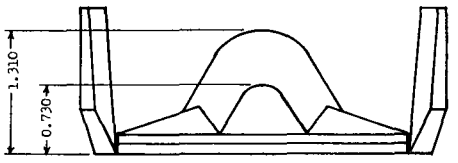

(a) Complete configuration and wing-section details.

Figure 1.- Model and component drawings. All linear dimensions are in inches.

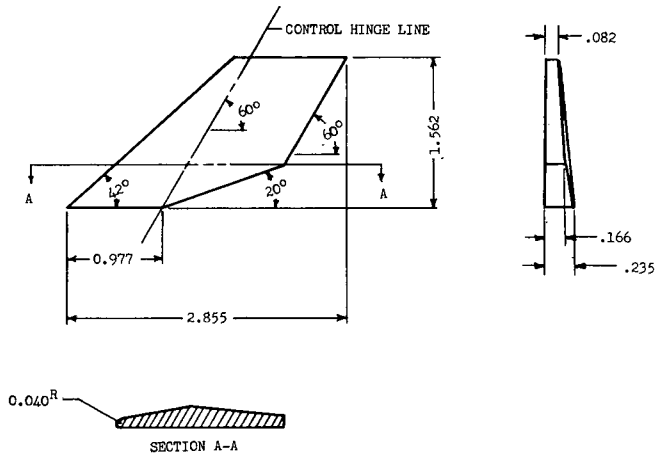

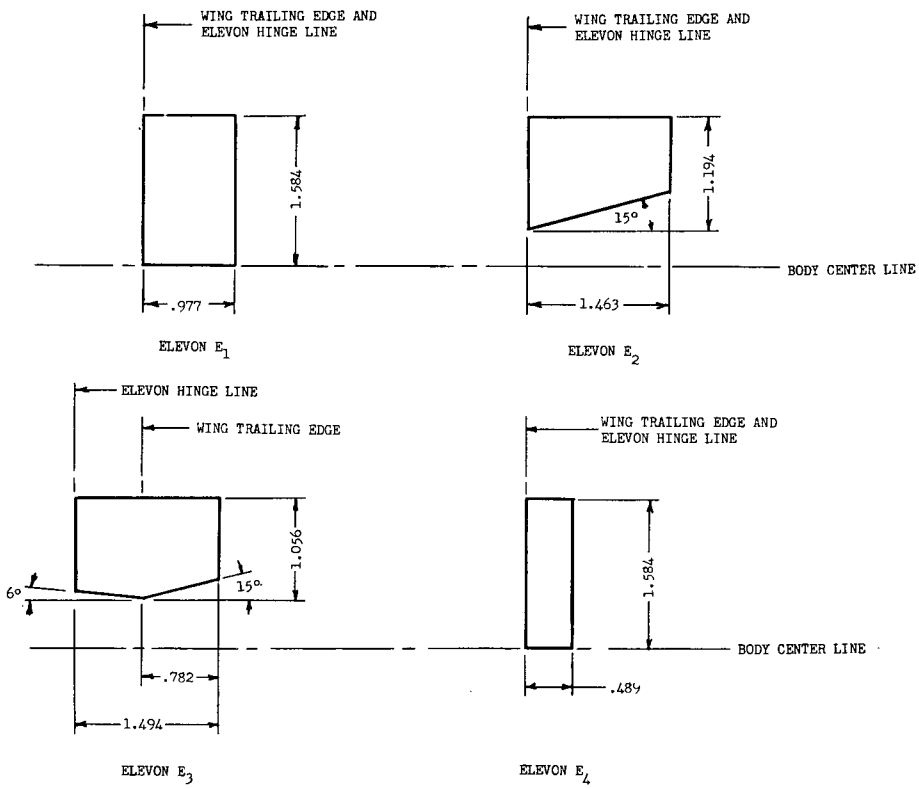

(b) Details of vertical fin and elevons.

Figure 1.- Continued.

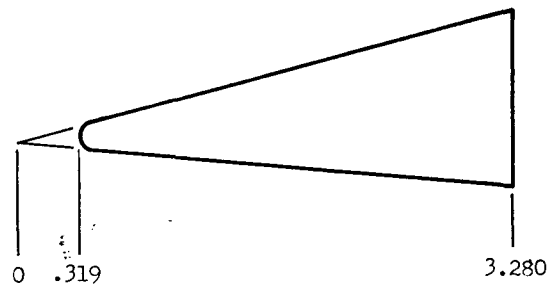

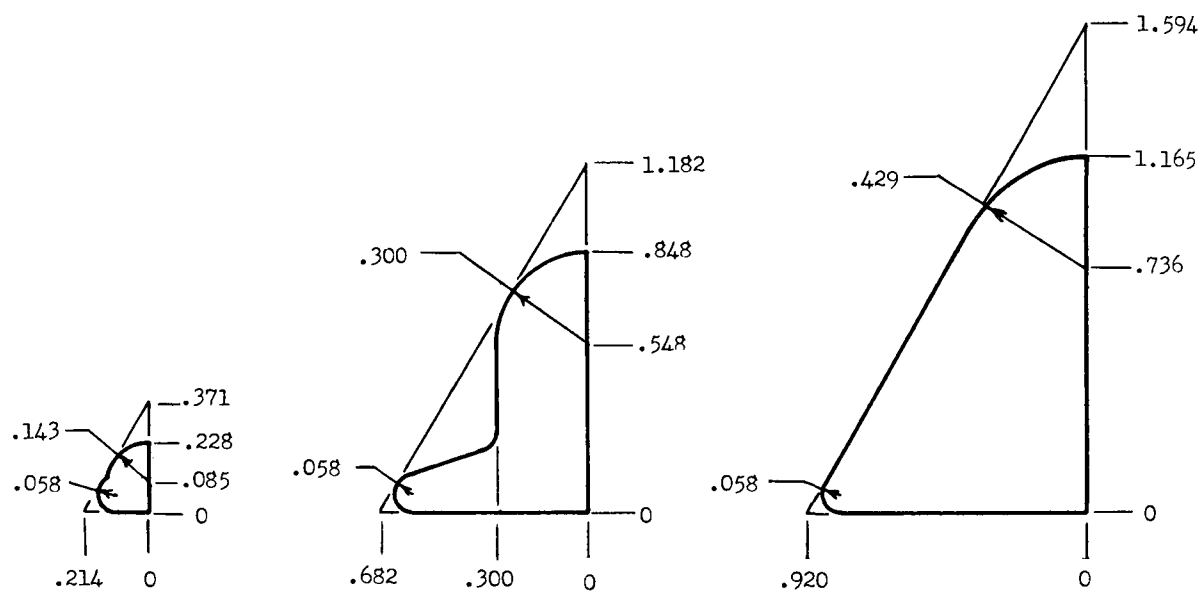

Station 0.641 Station 2.391 Station 3.280

(c) Details of modified nose.

Figure 1.- Concluded.

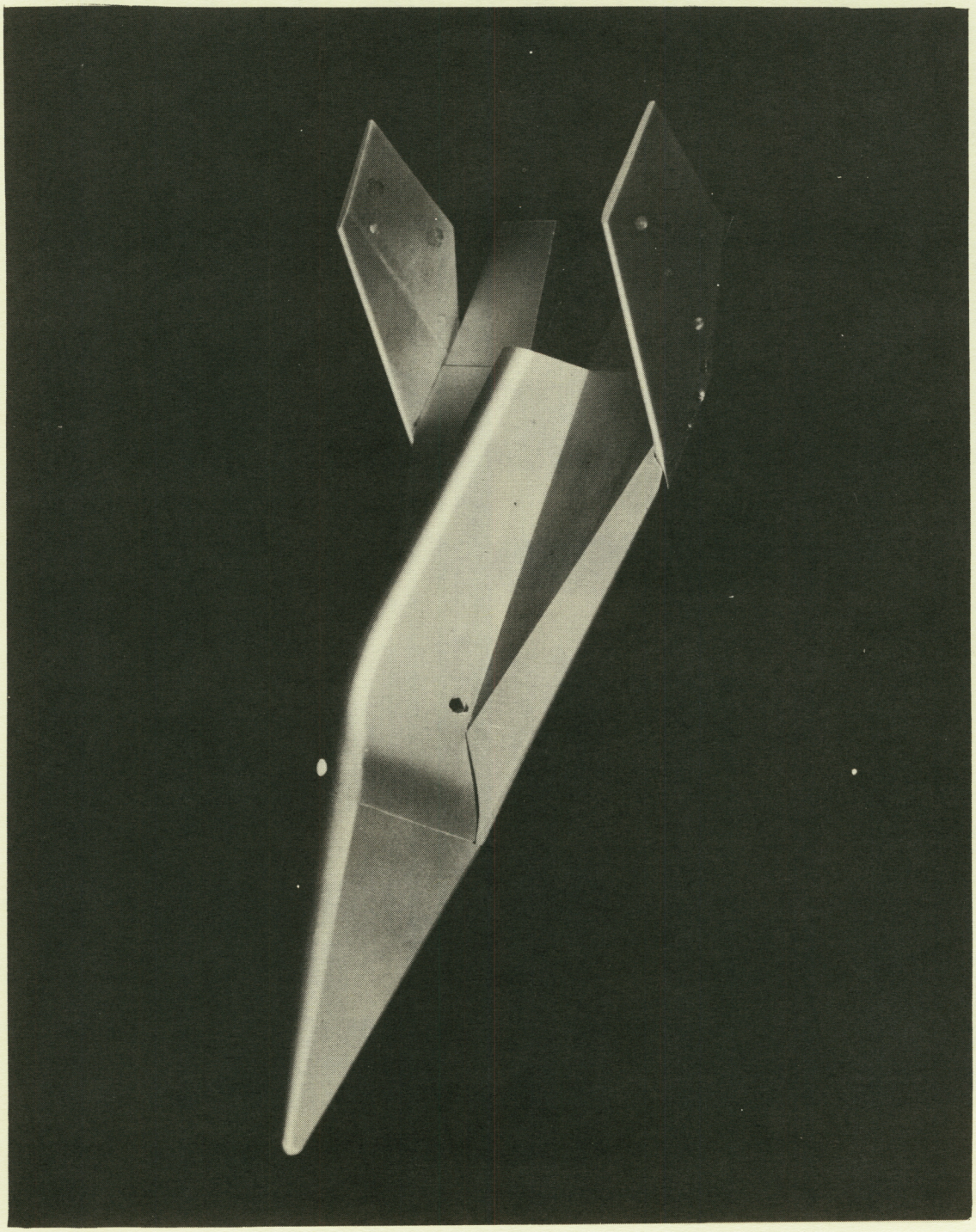

(a) Configuration BW_2E_2F. L-62-6383

Figure 2.- Model photographs.

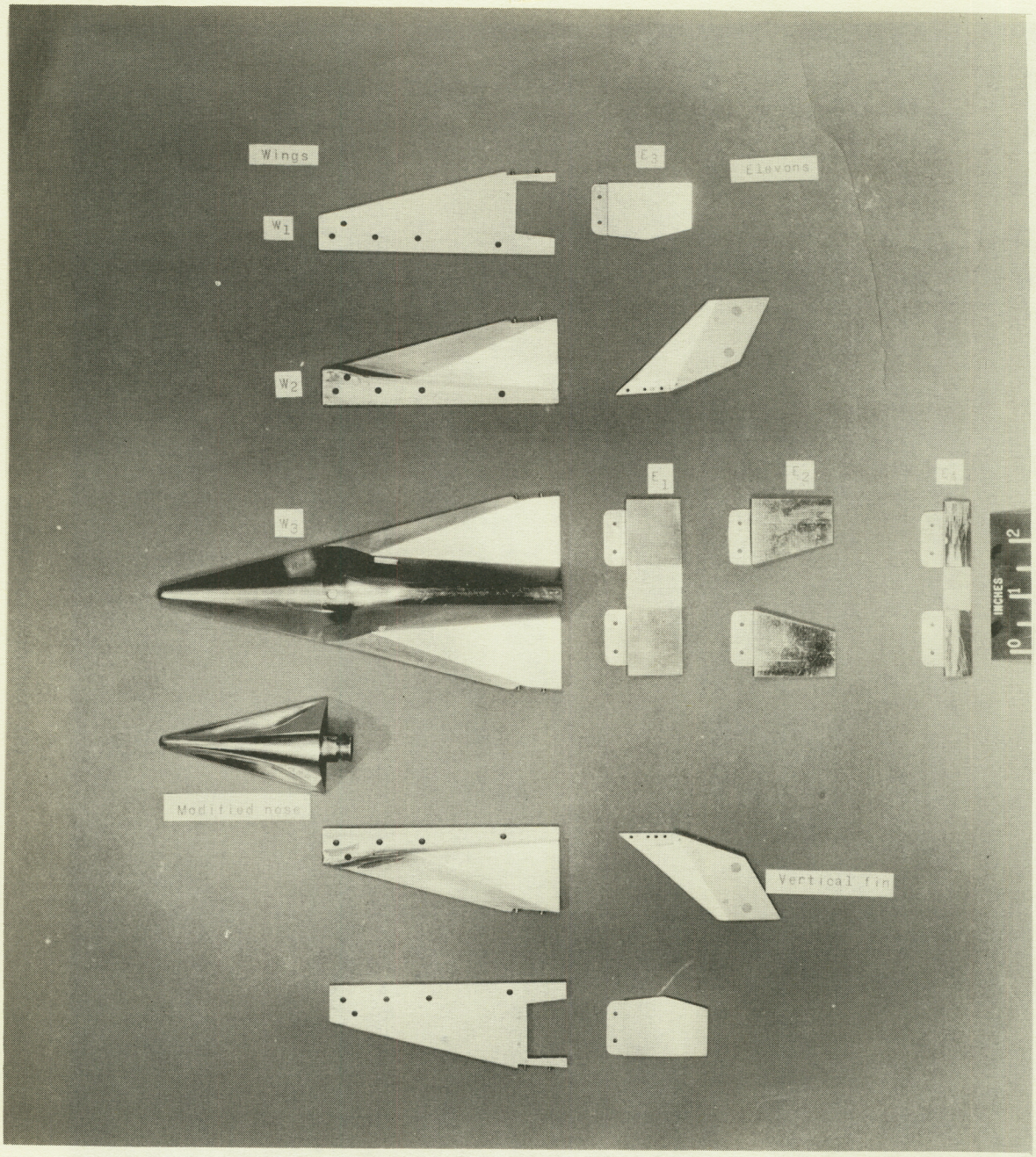

(b) Model components. L-62-8747

Figure 2.- Concluded.

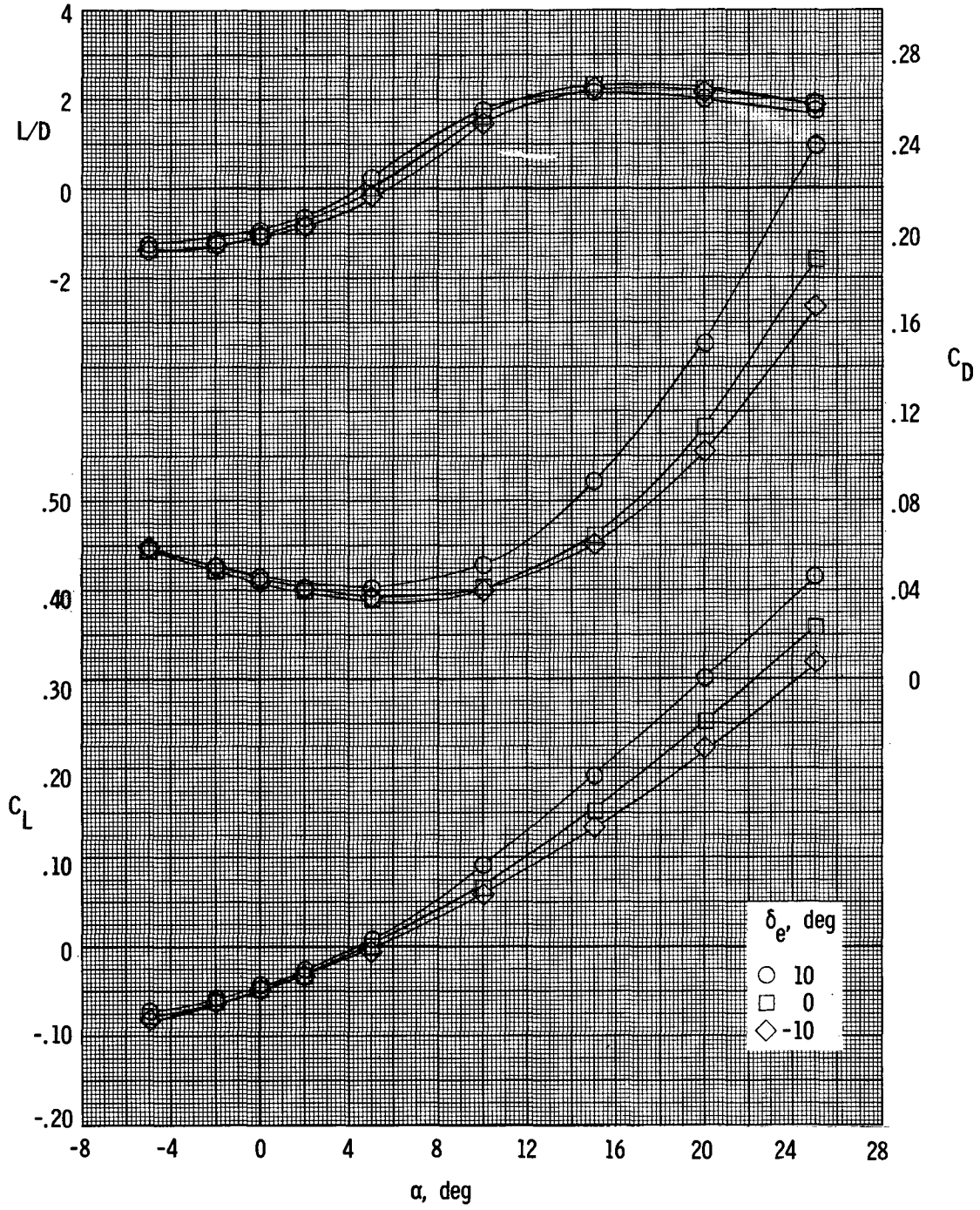

(a) Configuration BW_2E_1F.

Figure 3.- Longitudinal characteristics of configuration with E_1 and E_2 elevons on wing section W_2. $\delta_n = 0^o$; $\delta_r = 0^o$; M = 9.6.

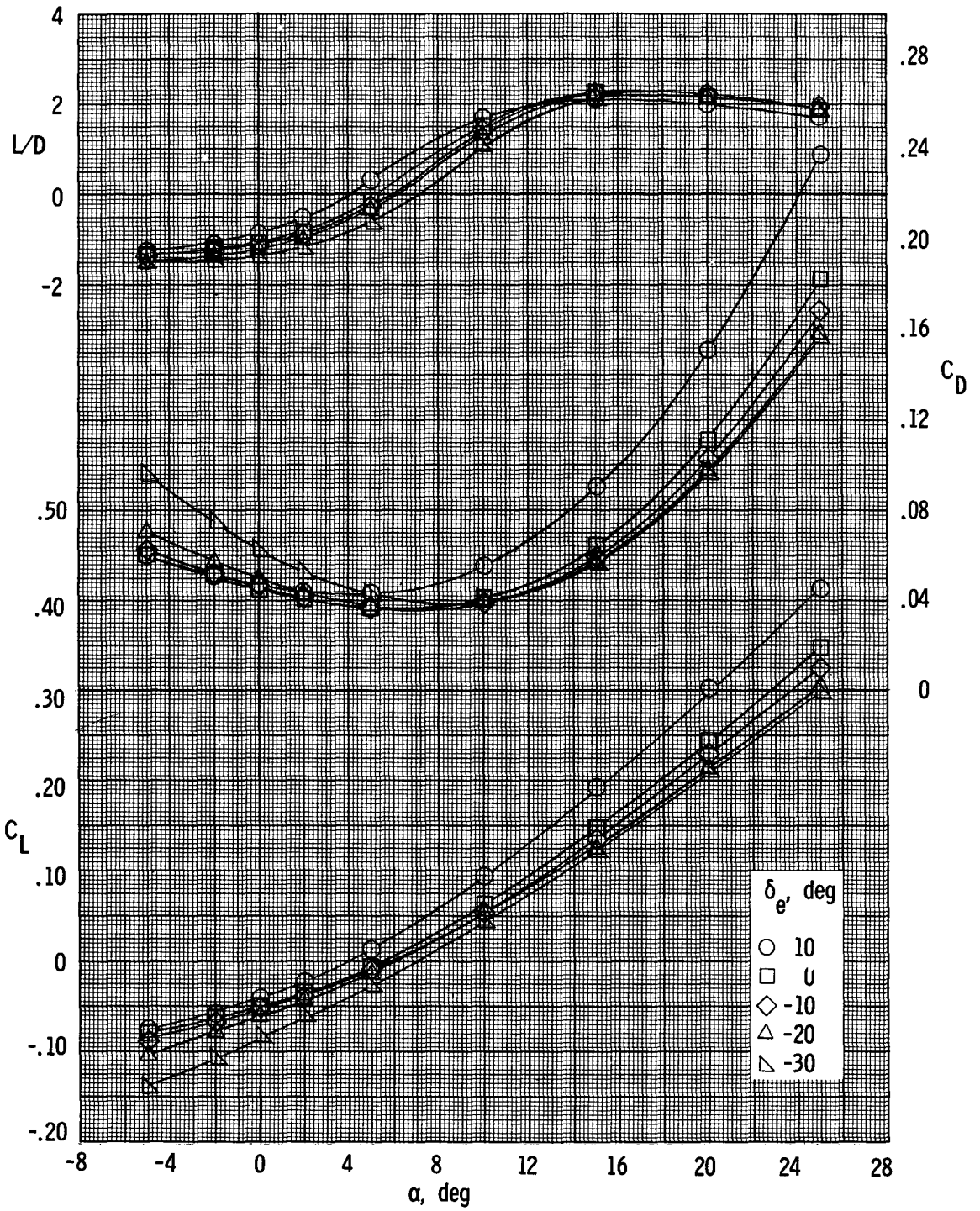

(b) Configuration BW_2E_2F.

Figure 3.- Continued.

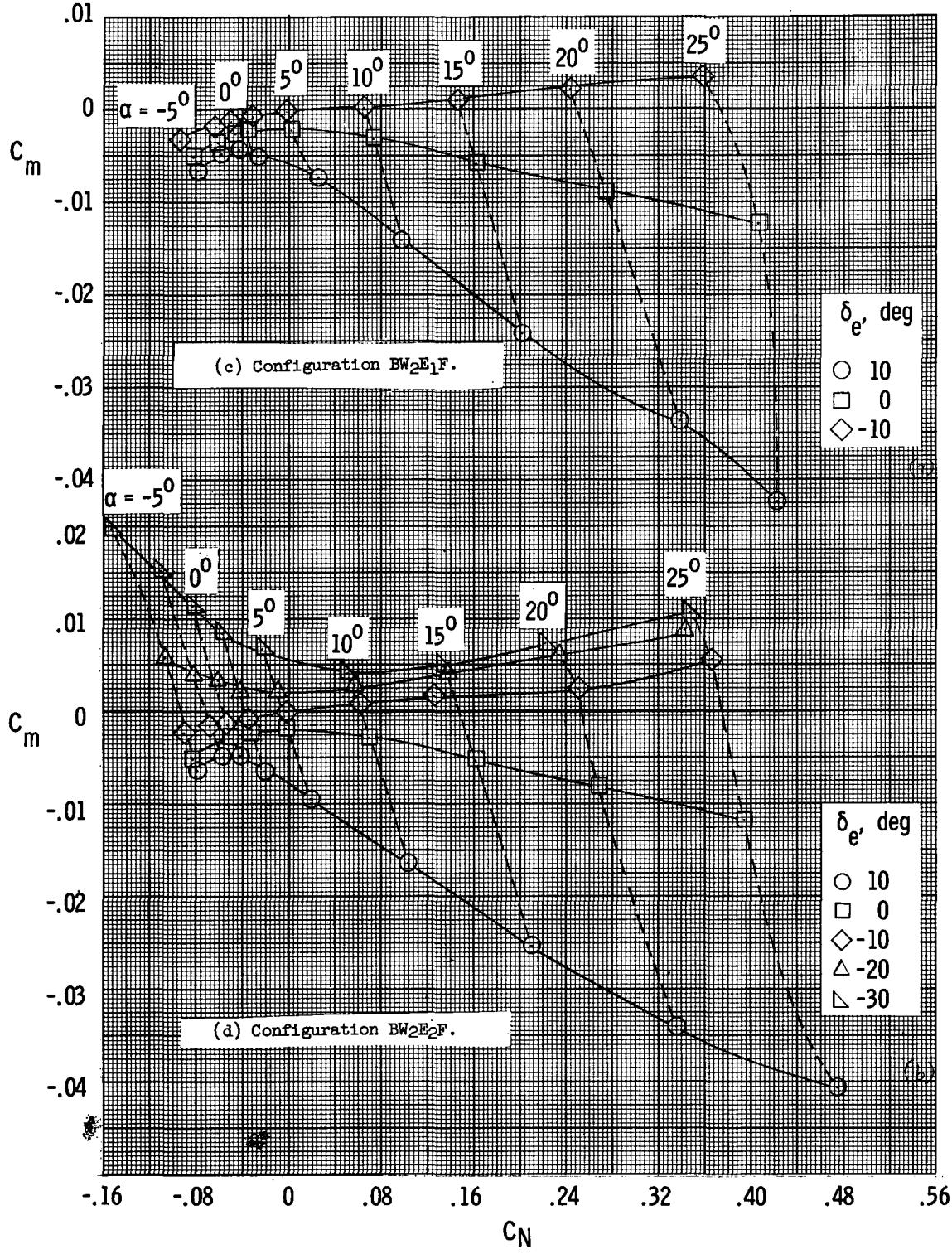

Figure 3.- Concluded.

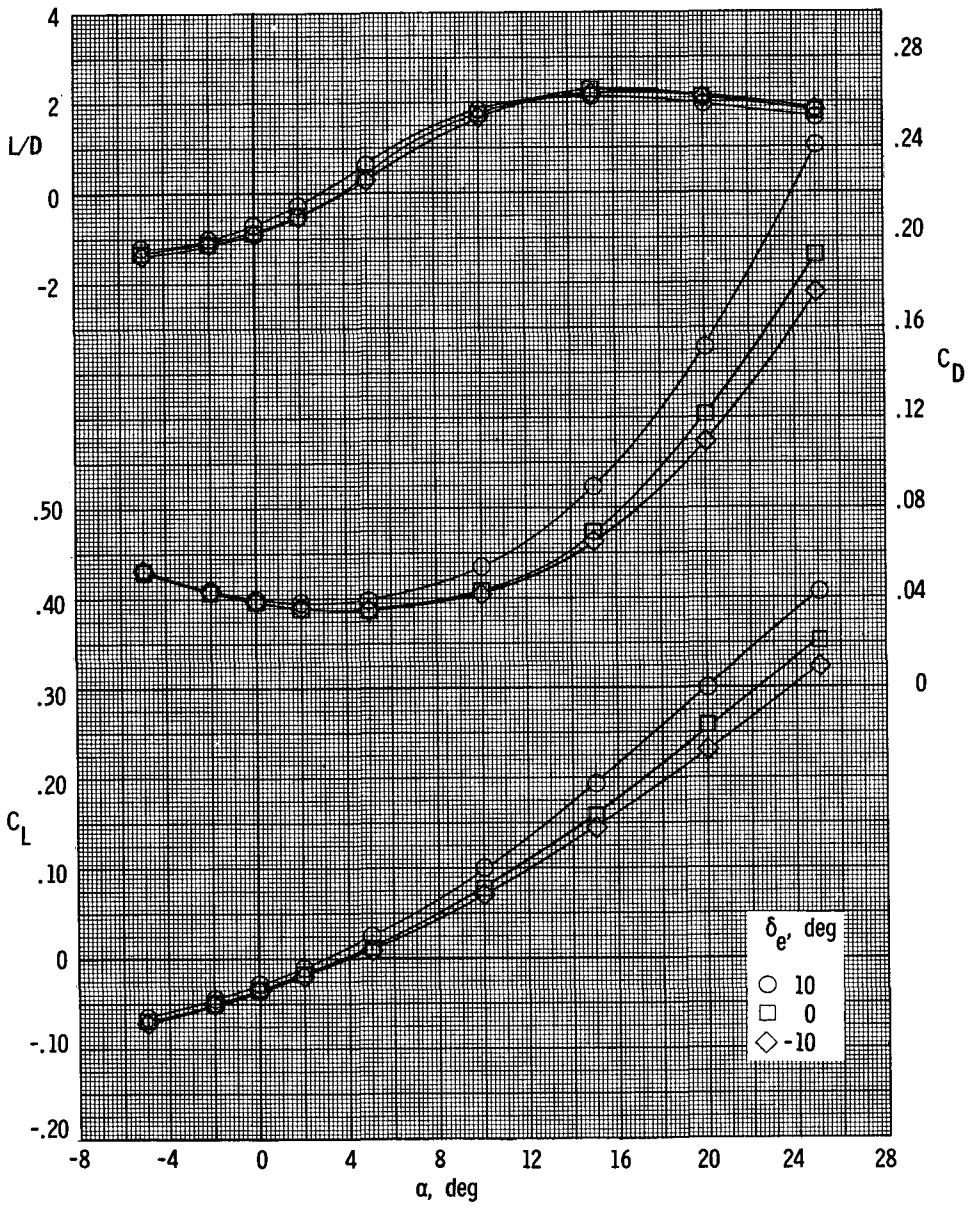

(a) Configuration BW_2E_1F.

Figure 4.- Longitudinal characteristics of configuration with E_1 and E_2 elevons on wing section W_2. $\delta_n = 5^\circ$; $\delta_r = 0^\circ$; M = 9.6.

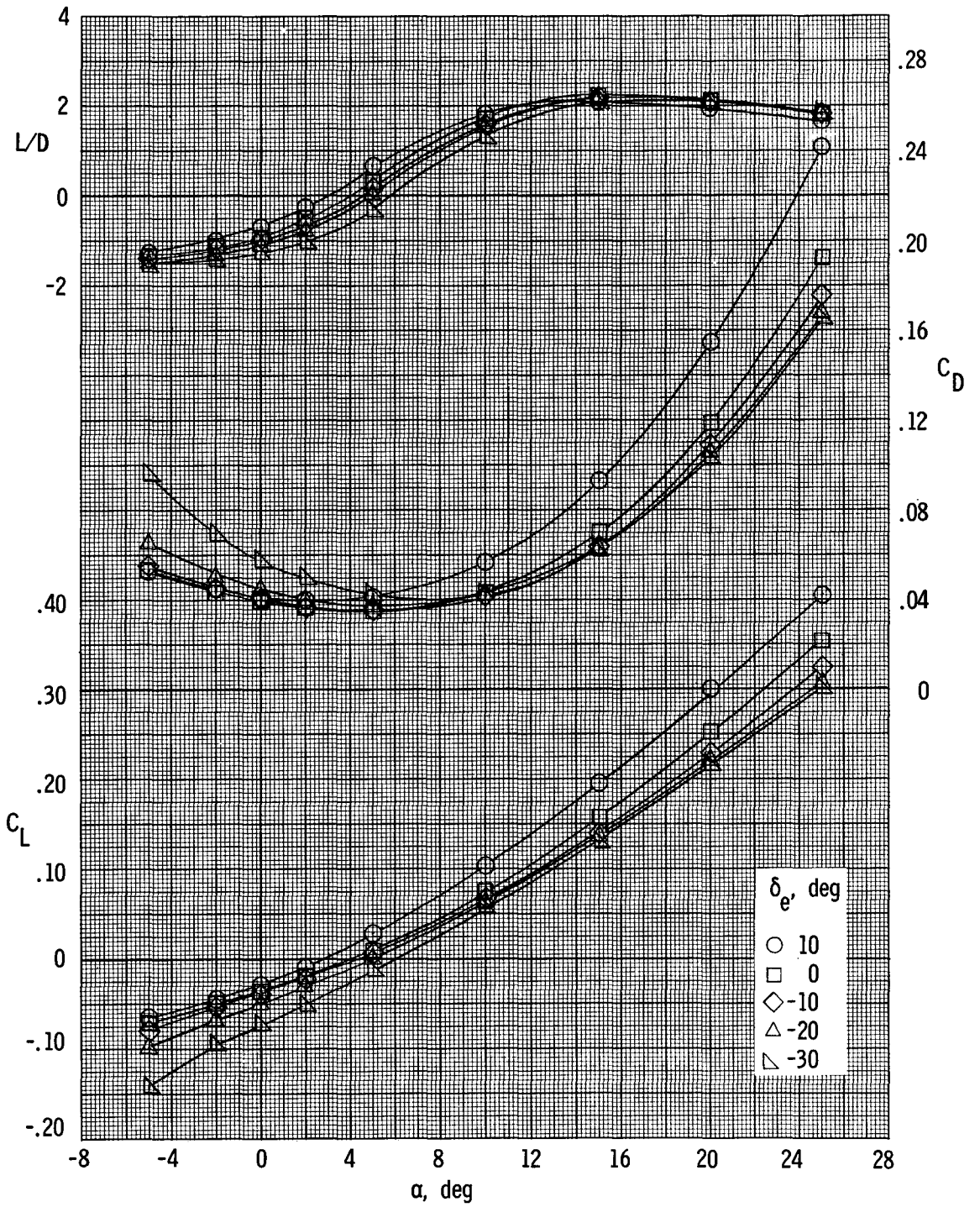

(b) Configuration BW_2E_2F.

Figure 4.- Continued.

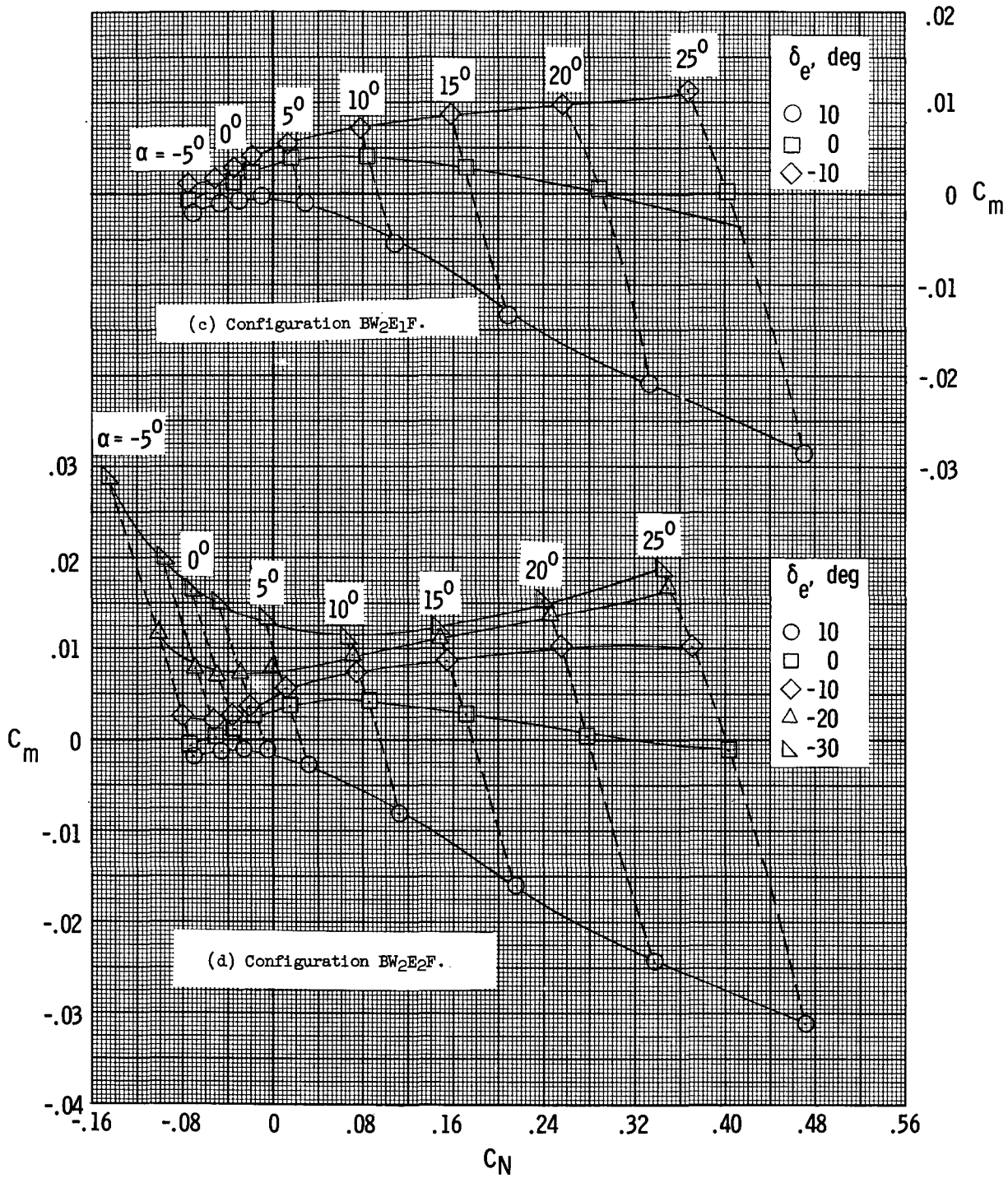

Figure 4.- Concluded.

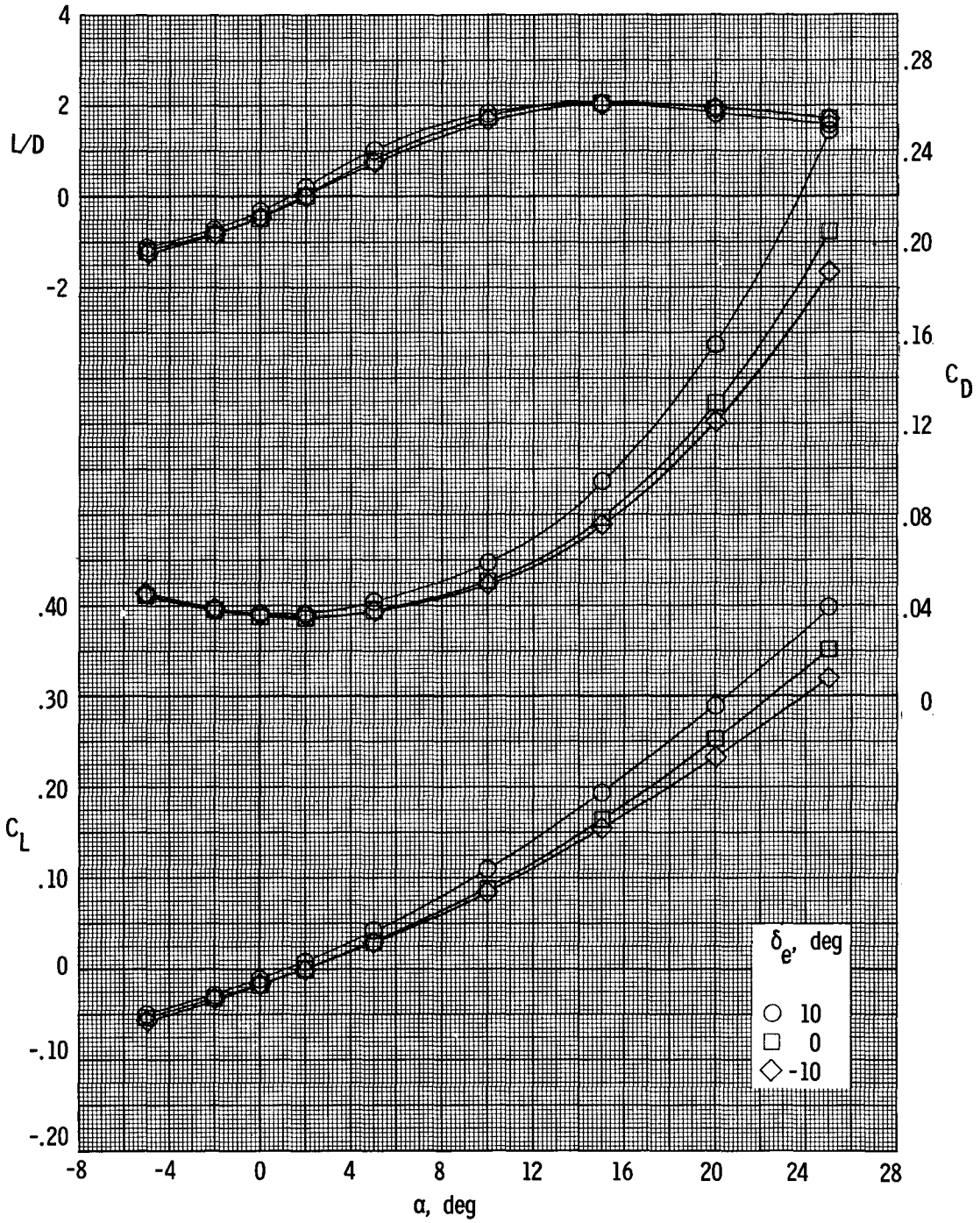

(a) Configuration BW_2E_1F.

Figure 5.- Longitudinal characteristics of configuration with E_1 and E_2 elevons on wing section W_2. $\delta_n = 10^o$; $\delta_r = 0^o$; M = 9.6.

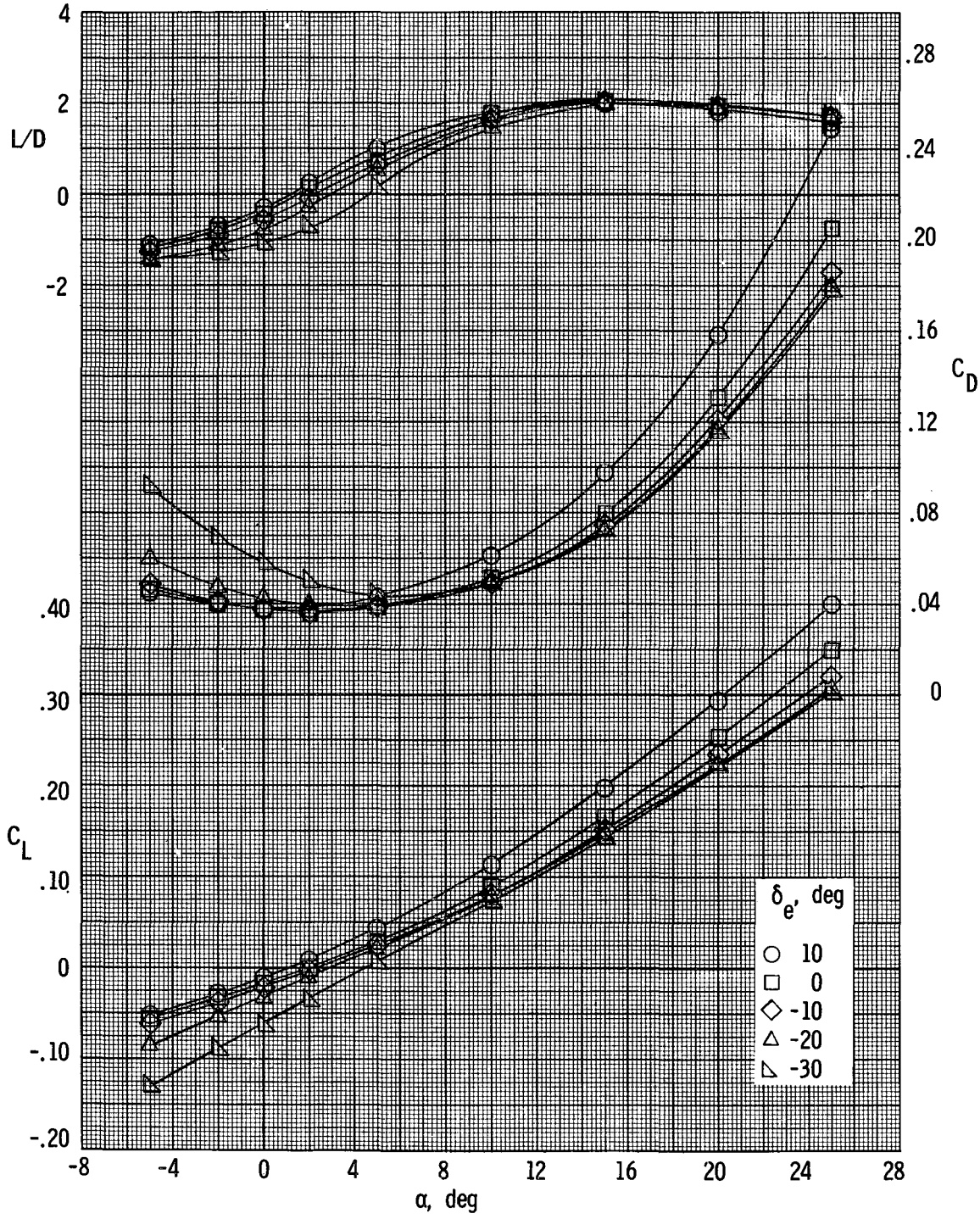

(b) Configuration BW_2E_2F.

Figure 5.- Continued.

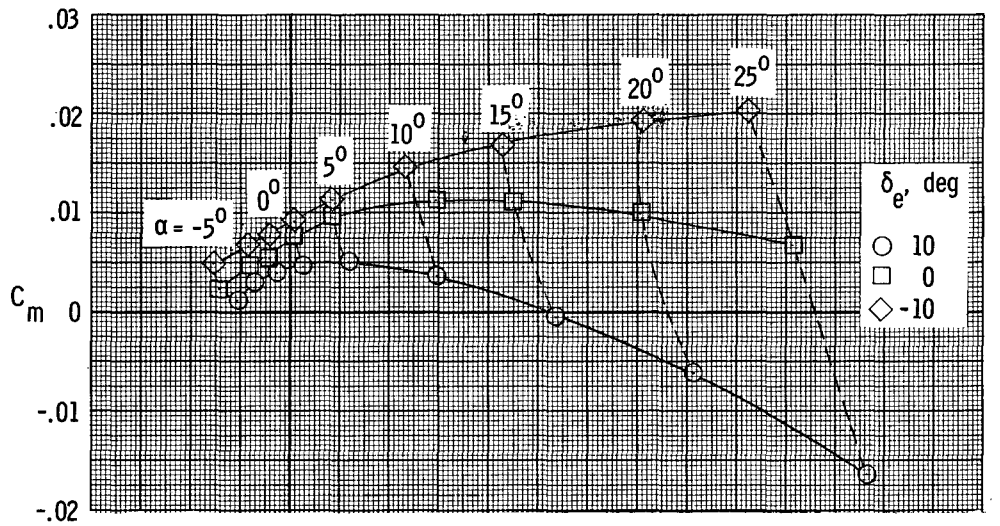

(c) Configuration BW_2E_1F.

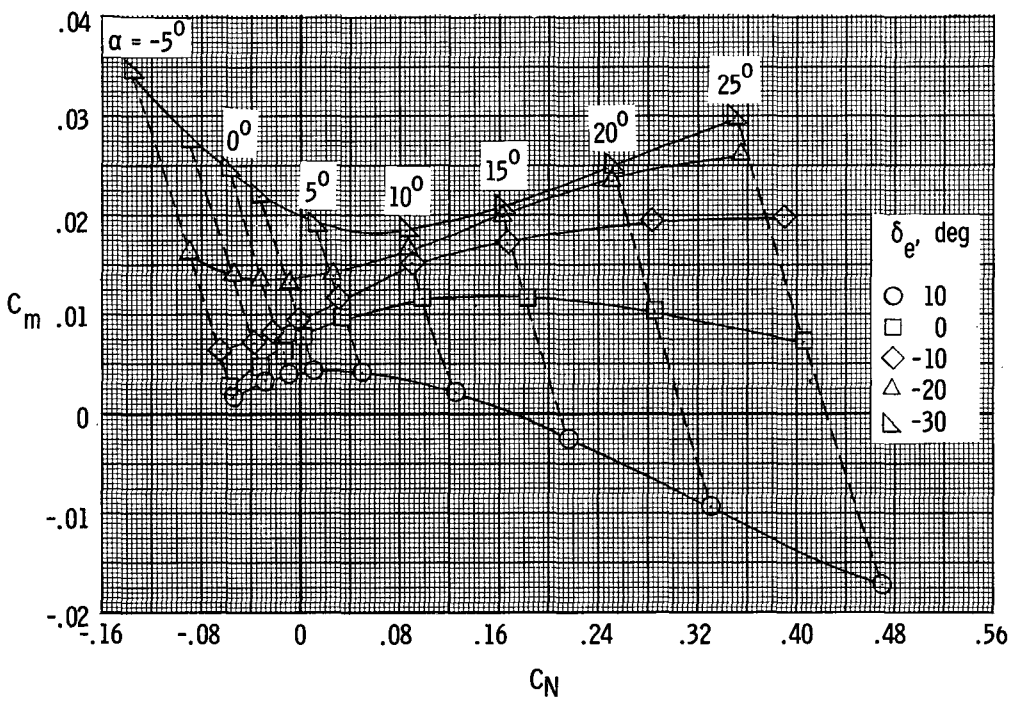

(d) Configuration BW_2E_2F.

Figure 5.- Concluded.

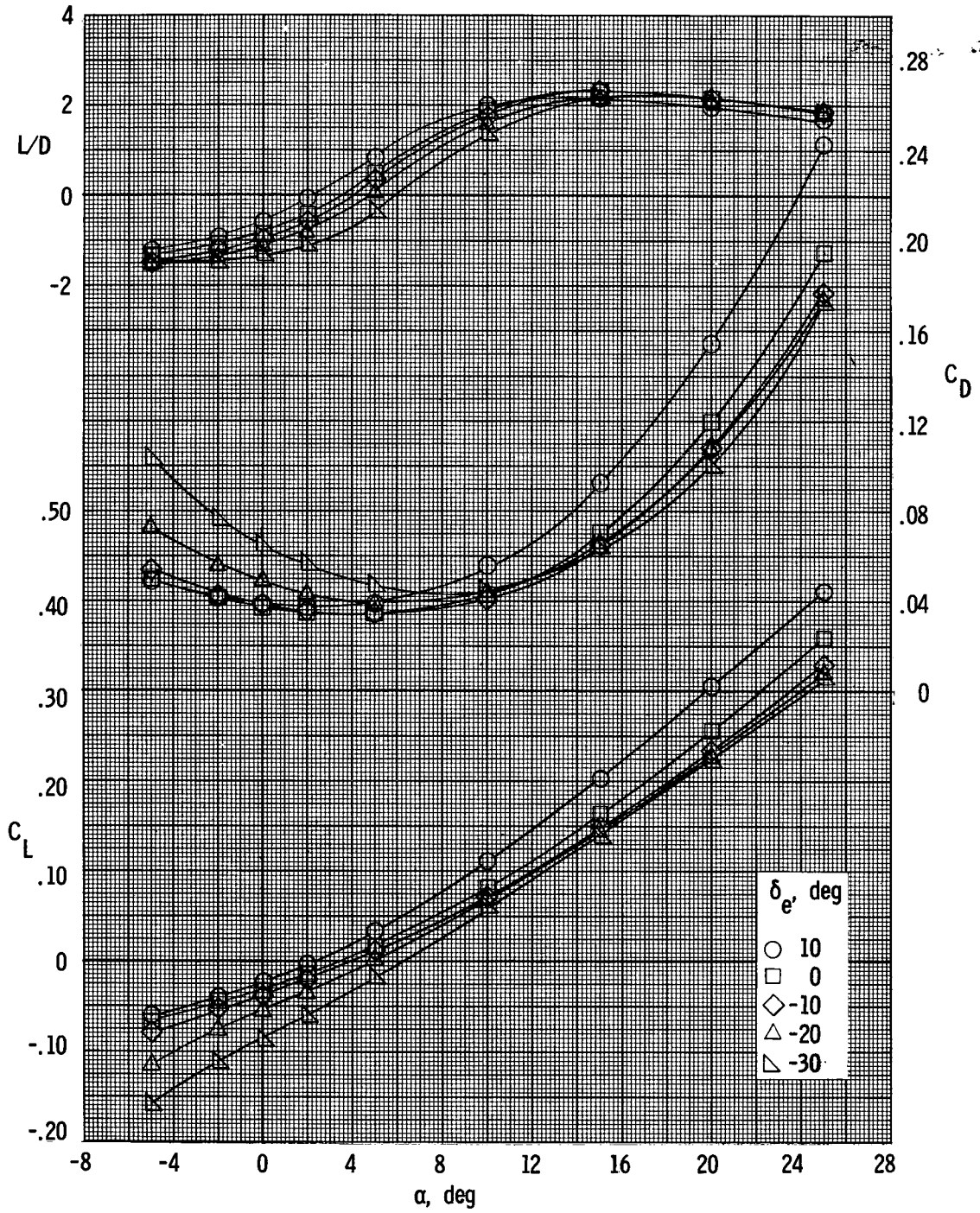

(a) Configuration BW_1E_2F.

Figure 6.- Longitudinal characteristics of configuration with E_2 and E_3 elevons on wing section W_1. $\delta_n = 5^o$; $\delta_r = 0^o$; M = 9.6.

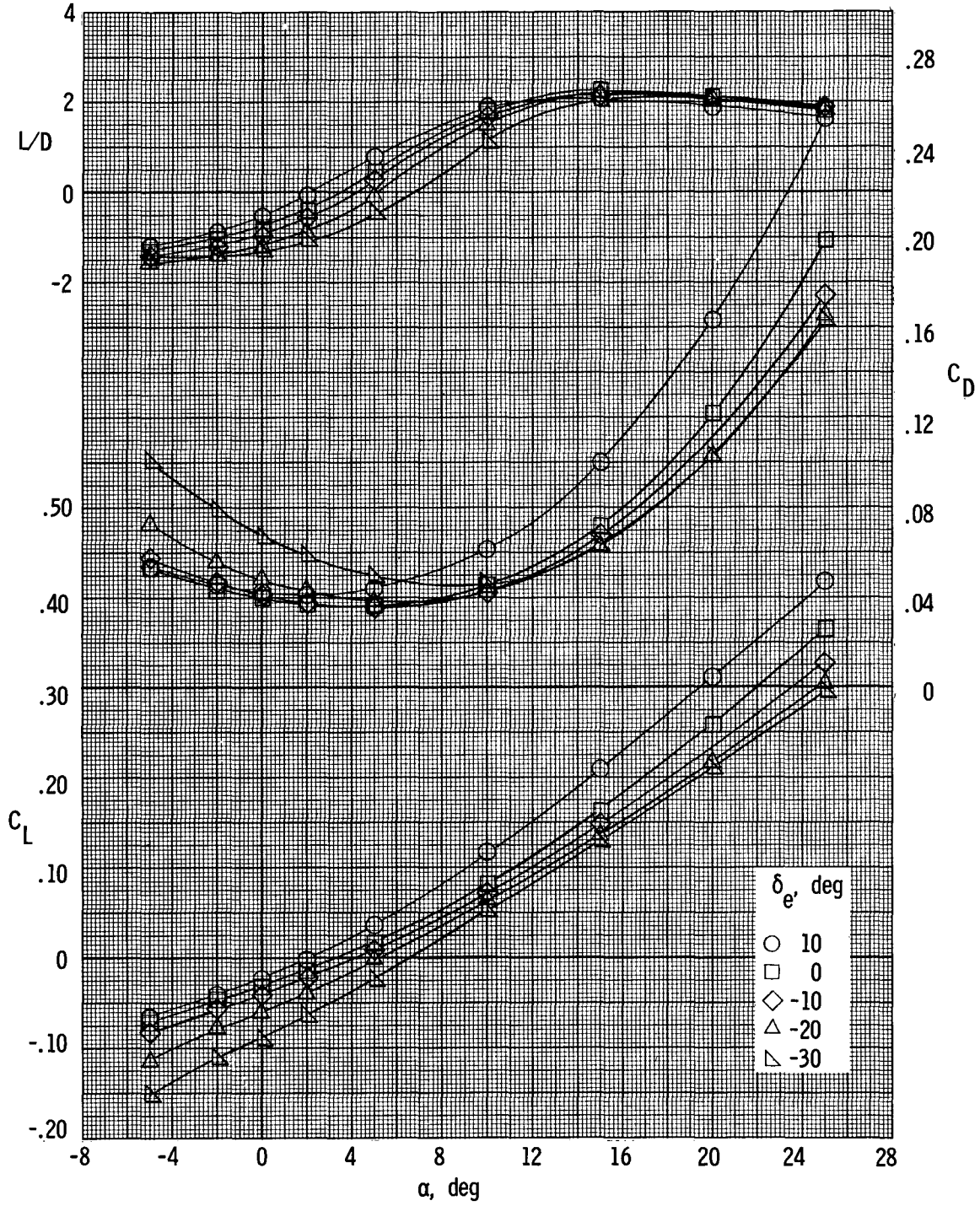

(b) Configuration BW_1E_3F.

Figure 6.- Continued.

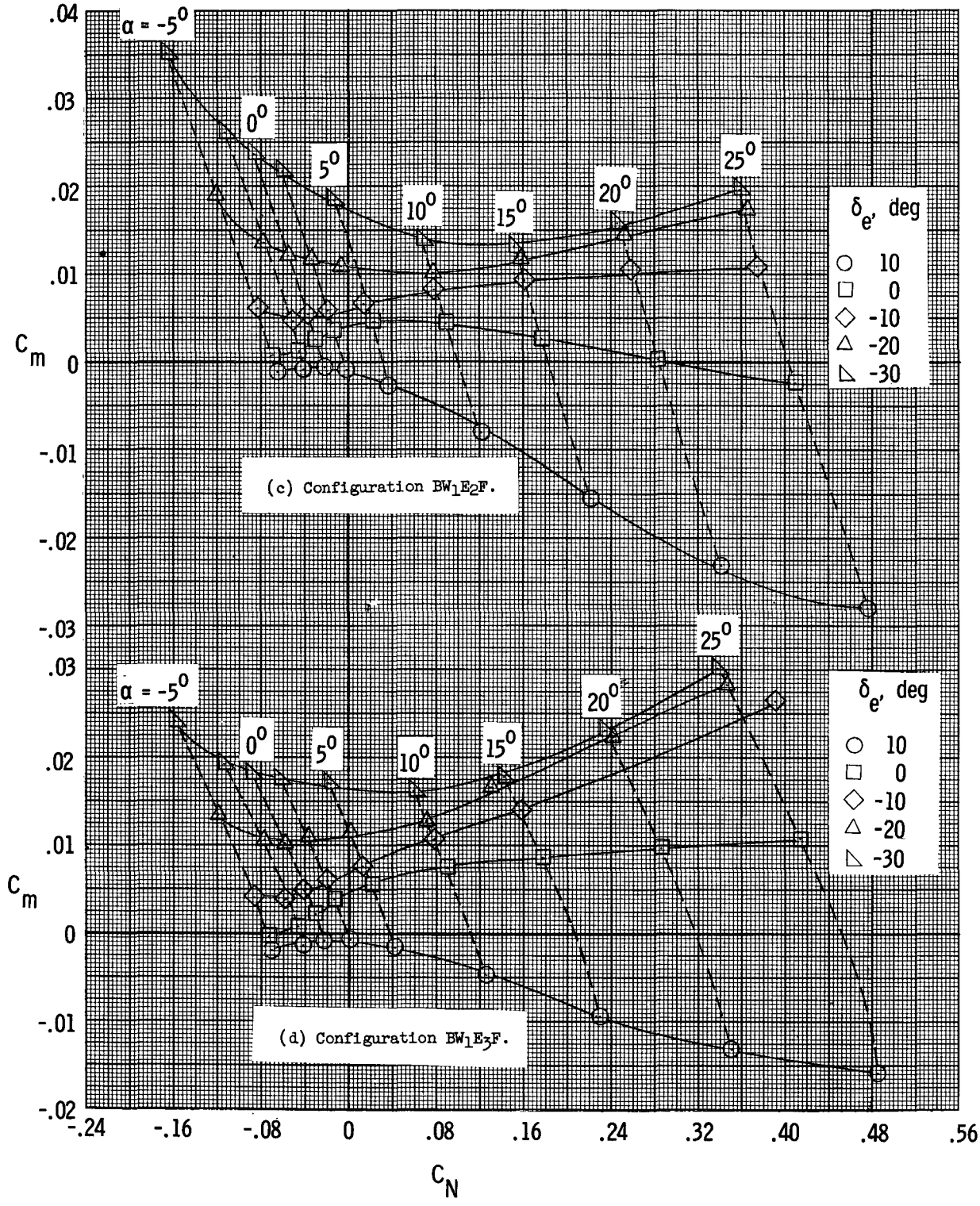

Figure 6.- Concluded.

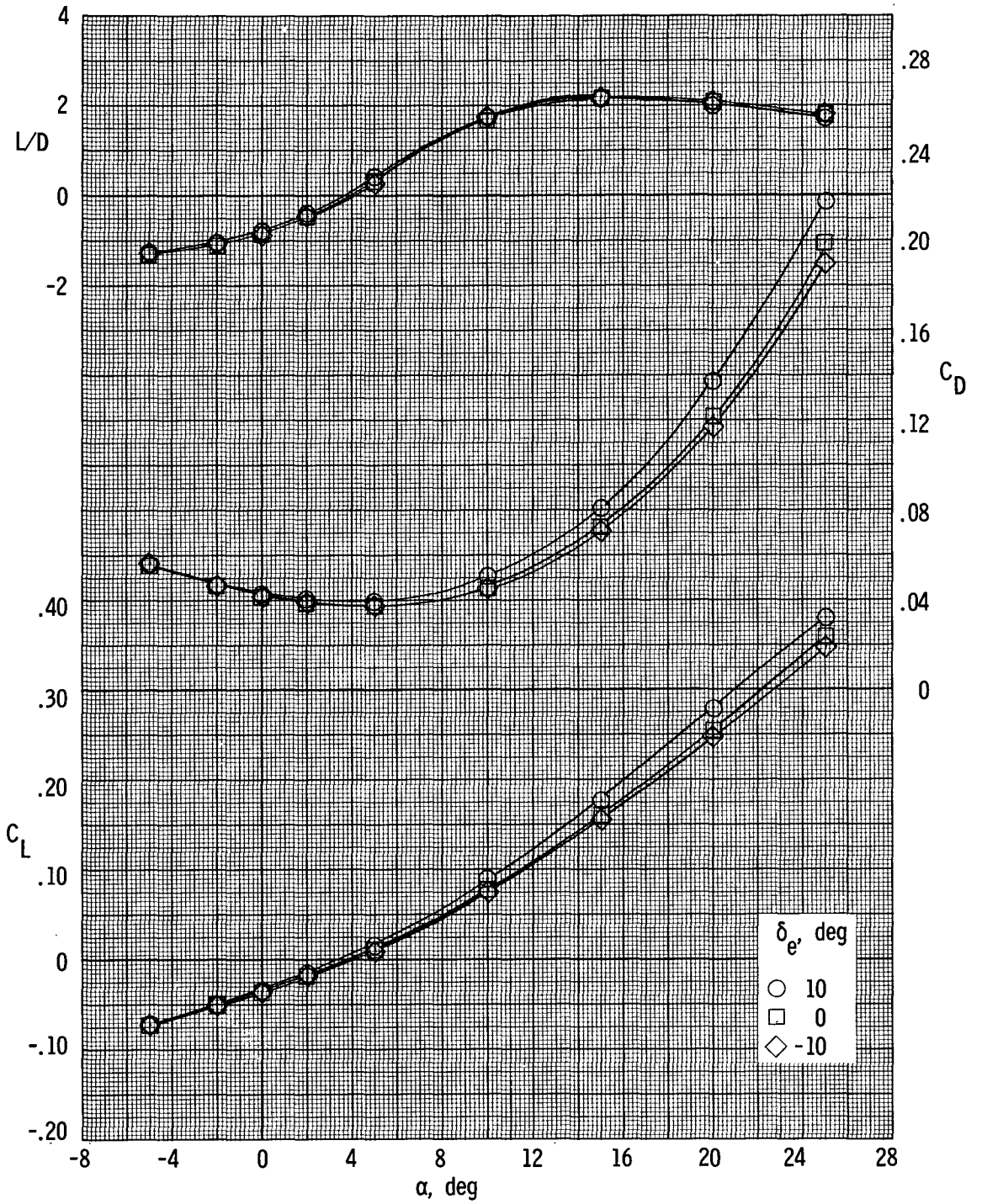

(a) Performance data.

Figure 7.- Longitudinal characteristics of configuration BW_2E_4F. $\delta_n = 5^o$; $\delta_r = 0^o$; M = 9.6.

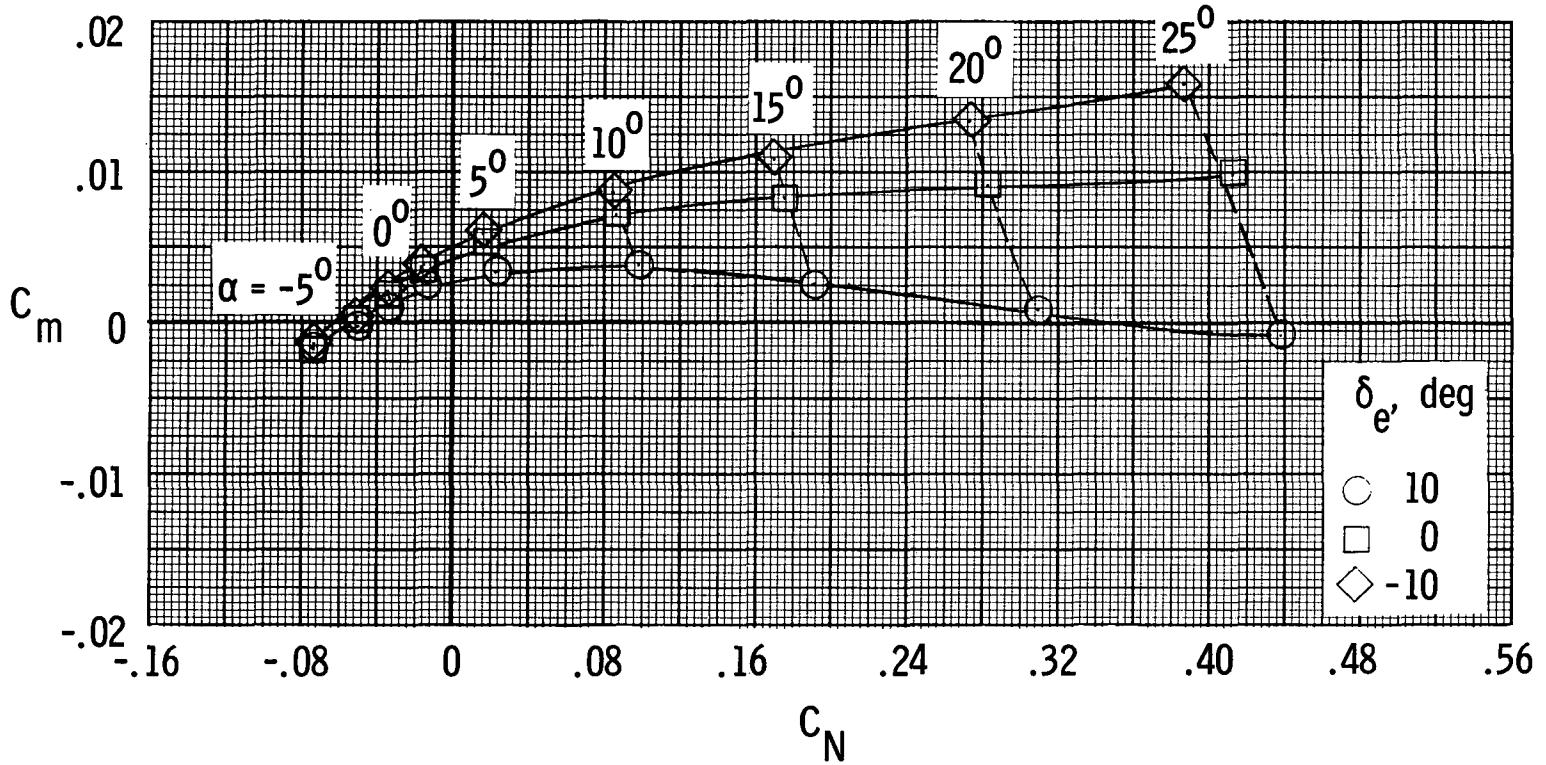

(b) Stability data.

Figure 7.- Concluded.

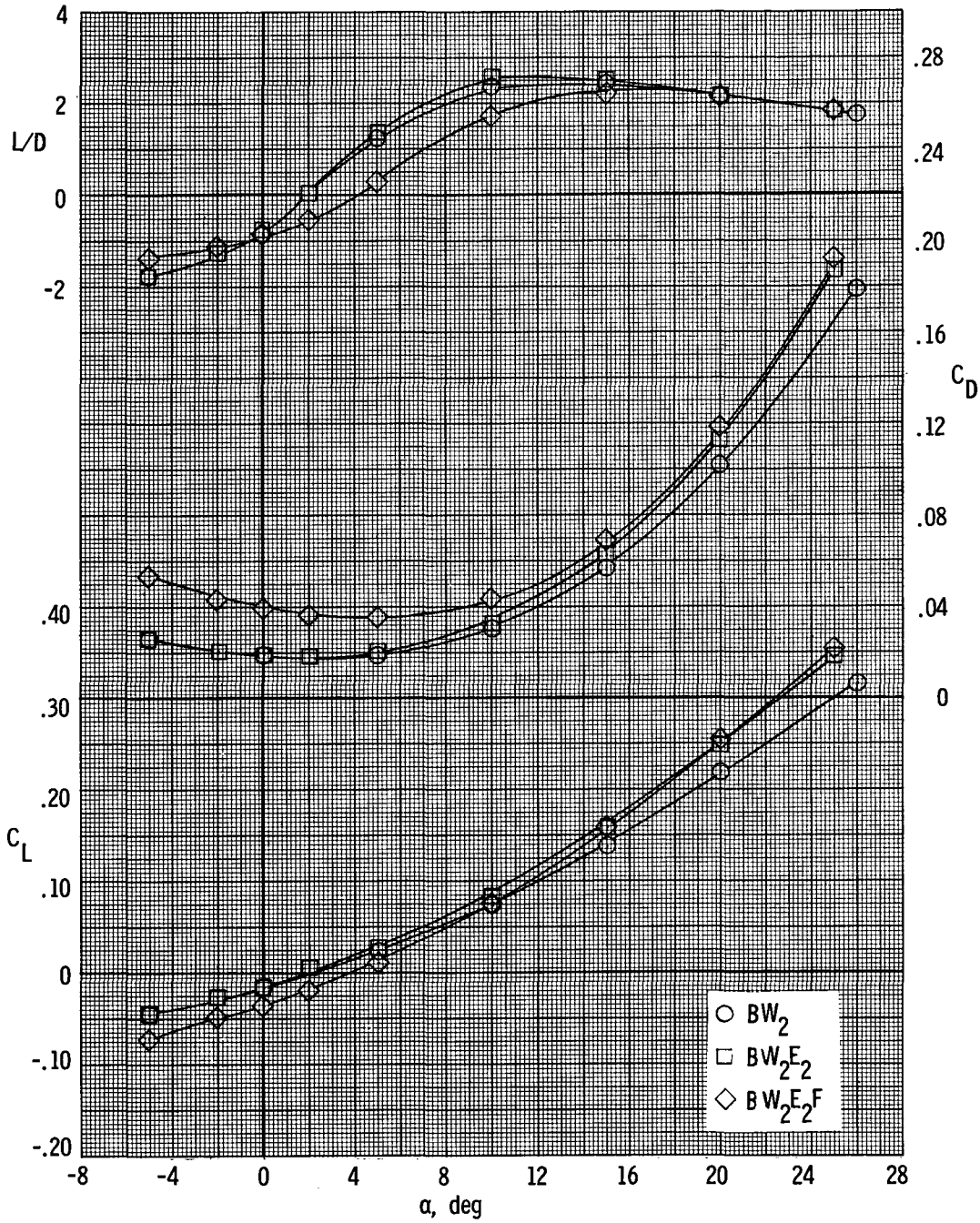

(a) Performance data.

Figure 8.- Effects of various model components on longitudinal characteristics. $\delta_n = 5^\circ$; $\delta_r = 0^\circ$; $\delta_e = 0^\circ$; M = 9.6.

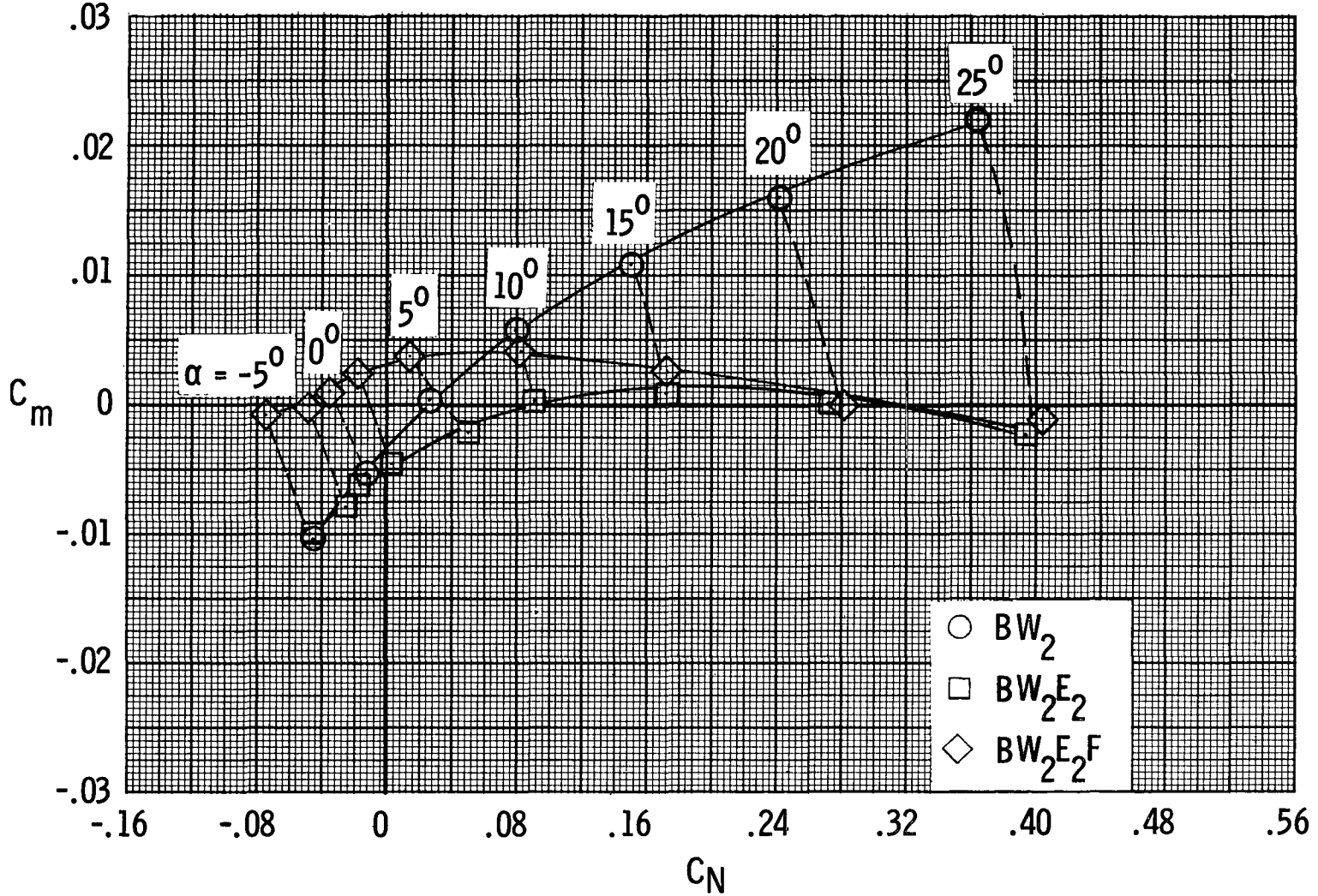

(b) Stability data.

Figure 8.- Concluded.

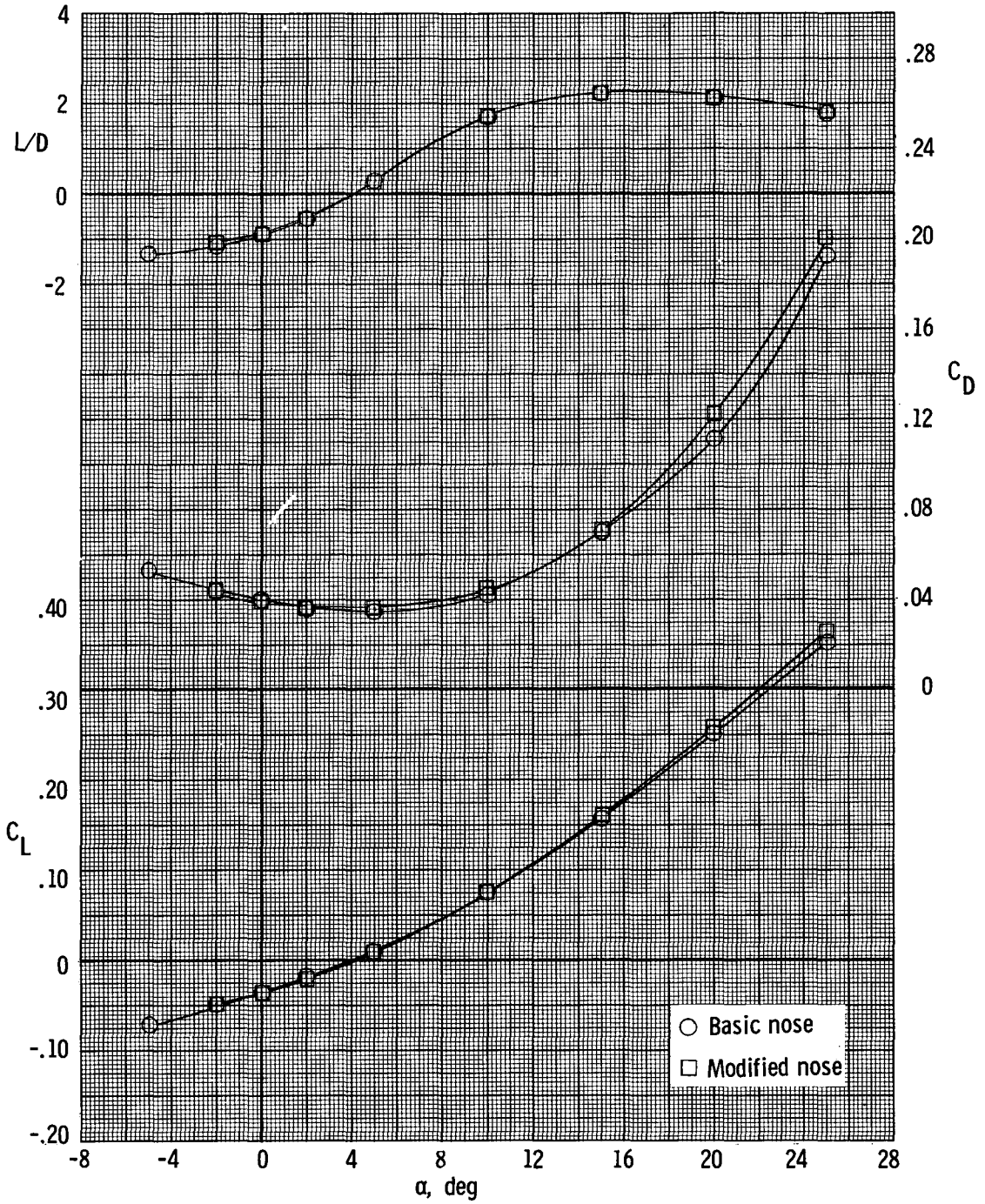

(a) Performance data on configuration BW_2E_2F.

Figure 9.- Effects of nose section and wing section on the longitudinal characteristics. $\delta_n = 5^o$; $\delta_r = 0^o$; $\delta_e = 0^o$; M = 9.6.

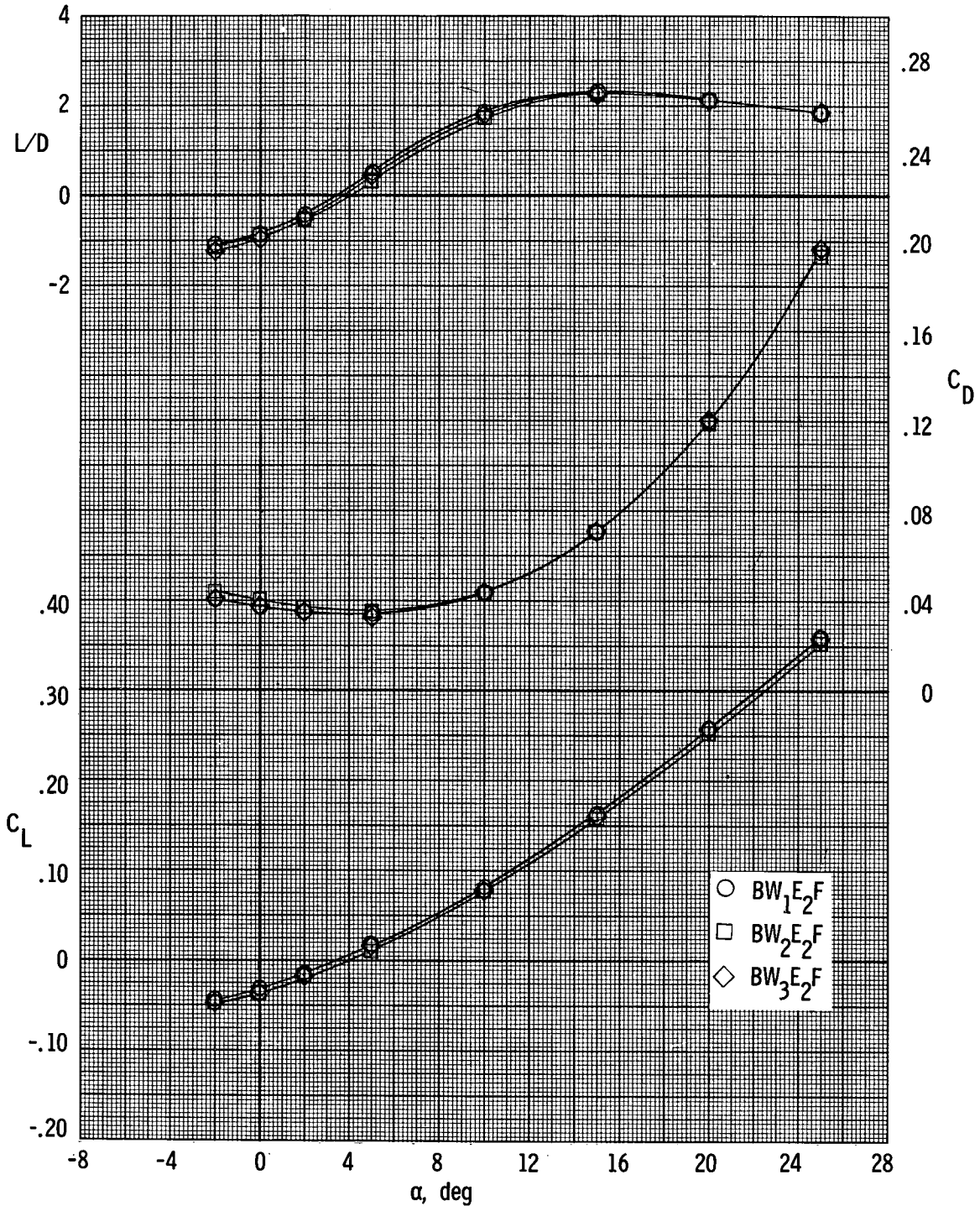

(b) Performance data.

Figure 9.- Continued.

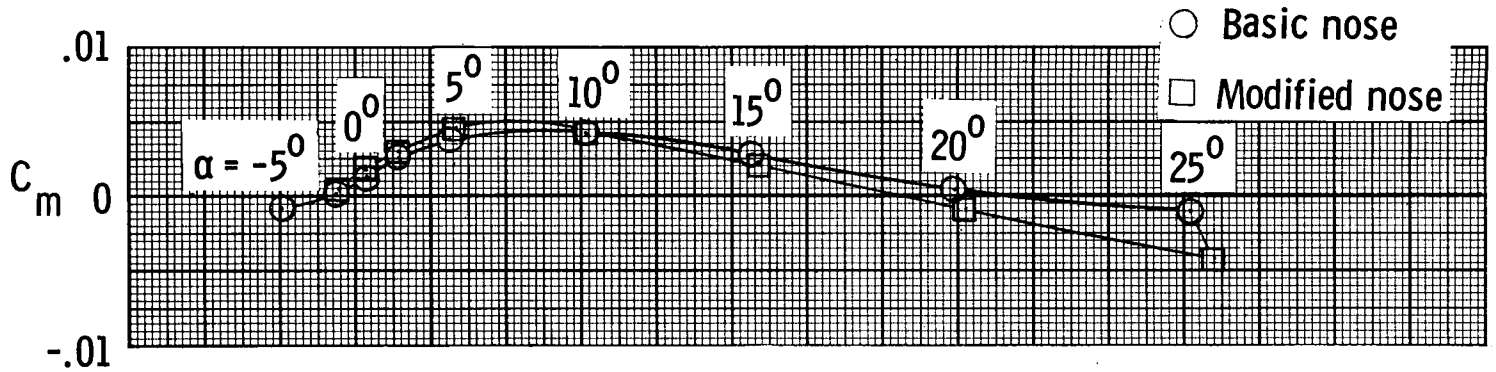

(c) Stability data for configuration BW_2E_2F.

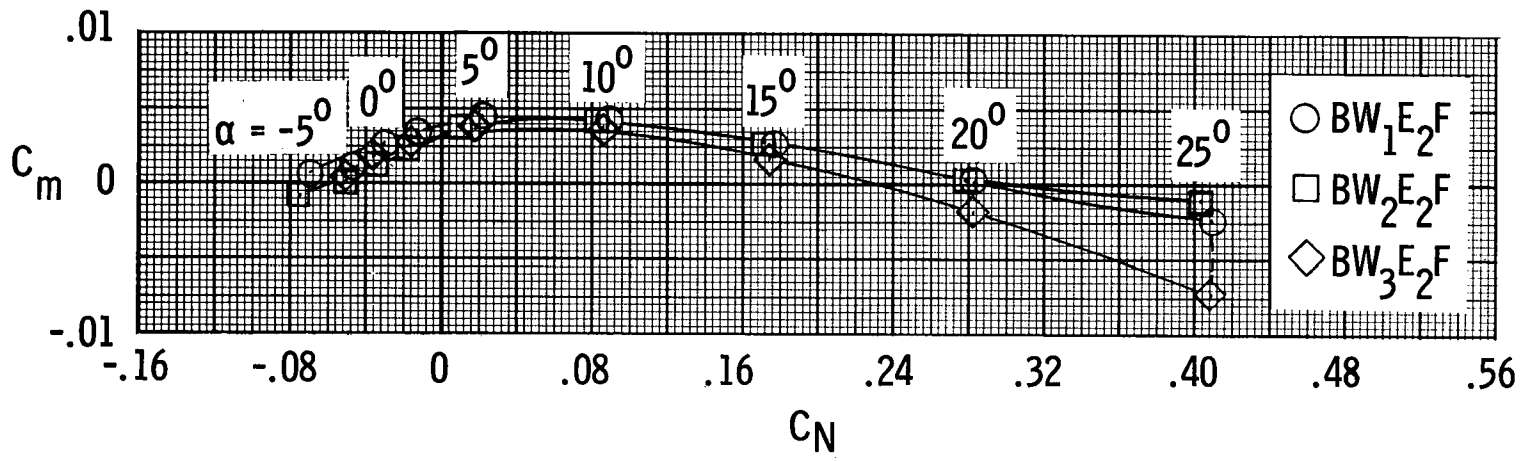

(d) Stability data.

Figure 9.- Concluded.

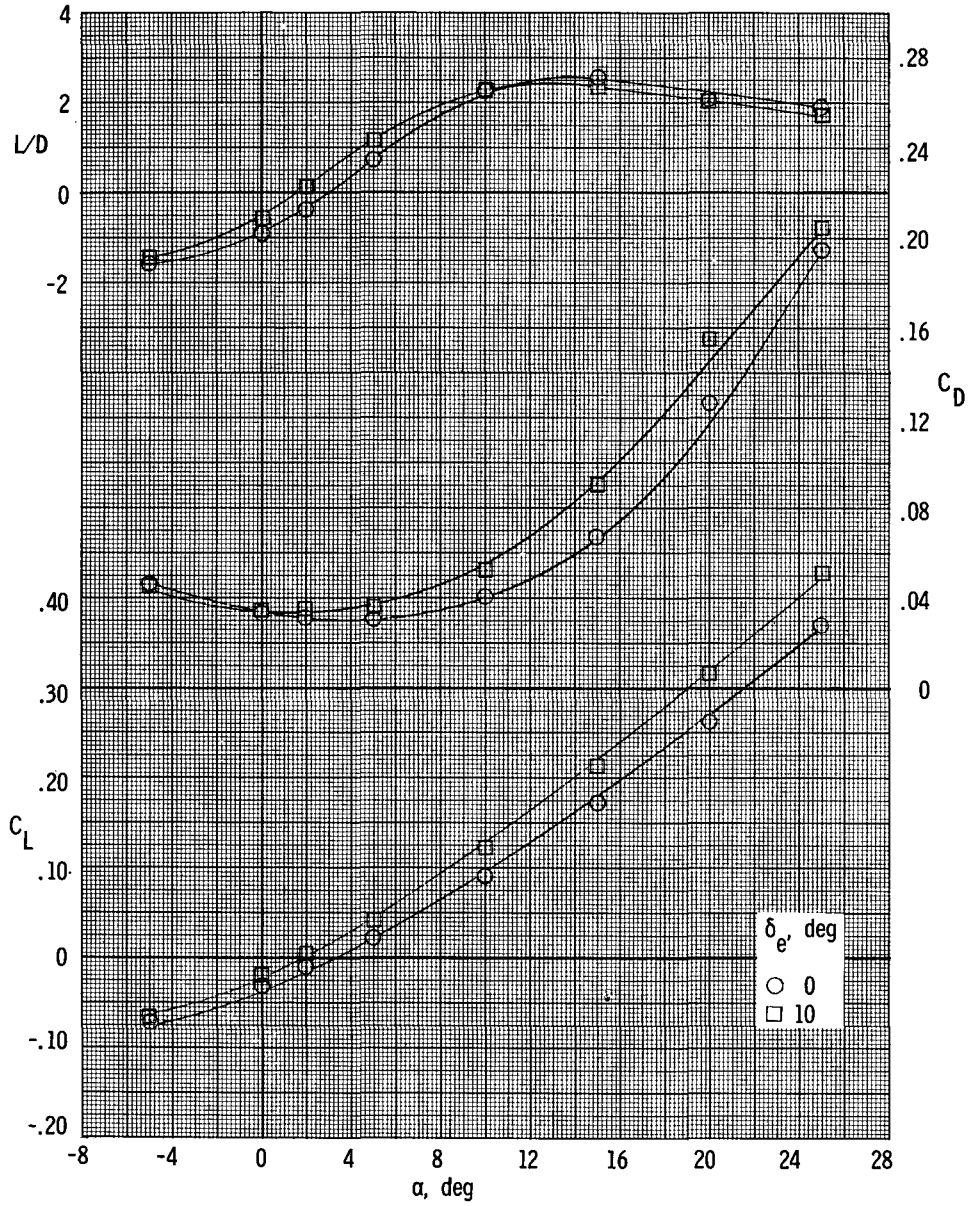

(a) Performance data.

Figure 10.- Longitudinal characteristics of configuration BW_2E_1F. $\delta_n = 5^o$; $\delta_r = 0^o$; M = 6.8.

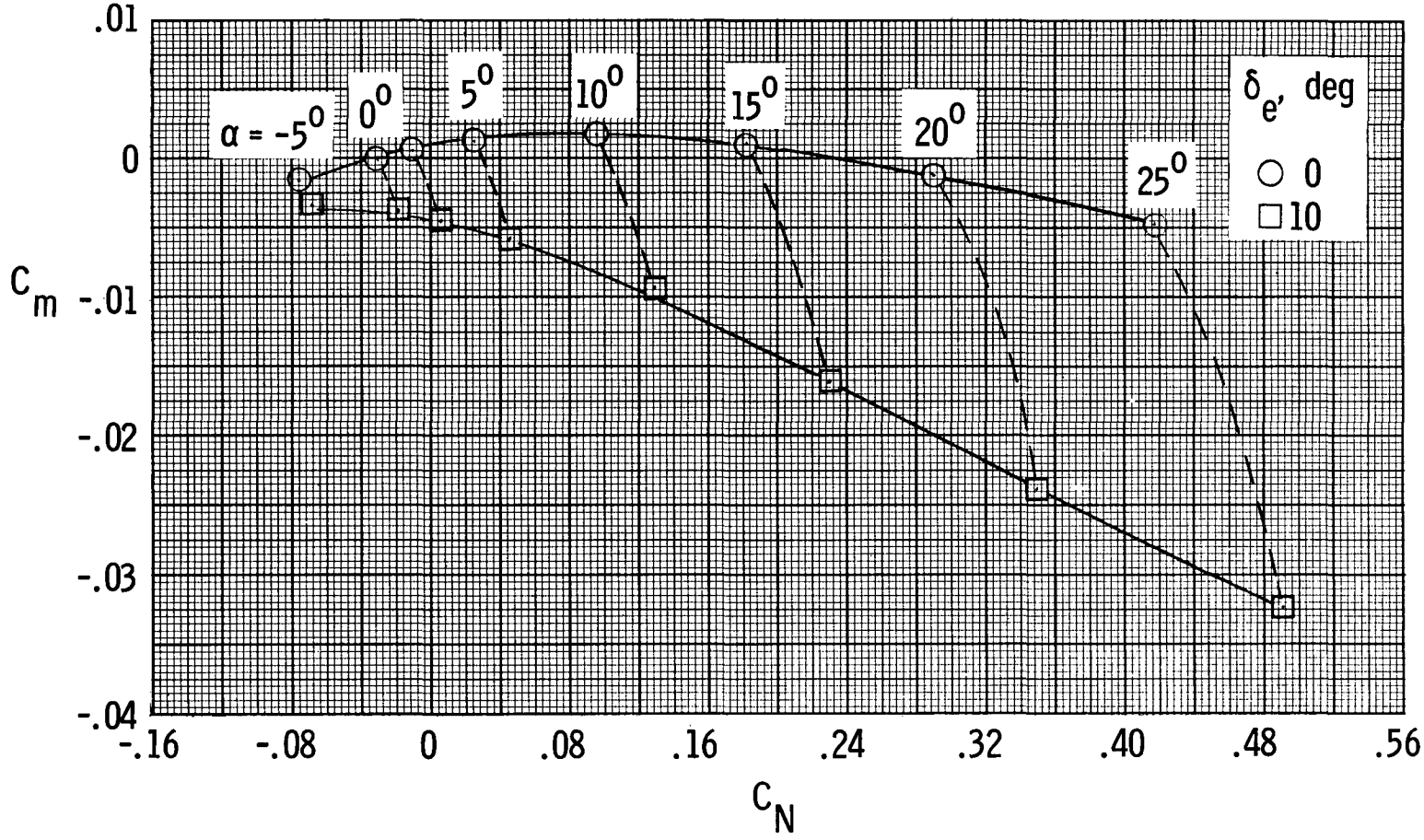

(b) Stability data.

Figure 10.- Concluded.

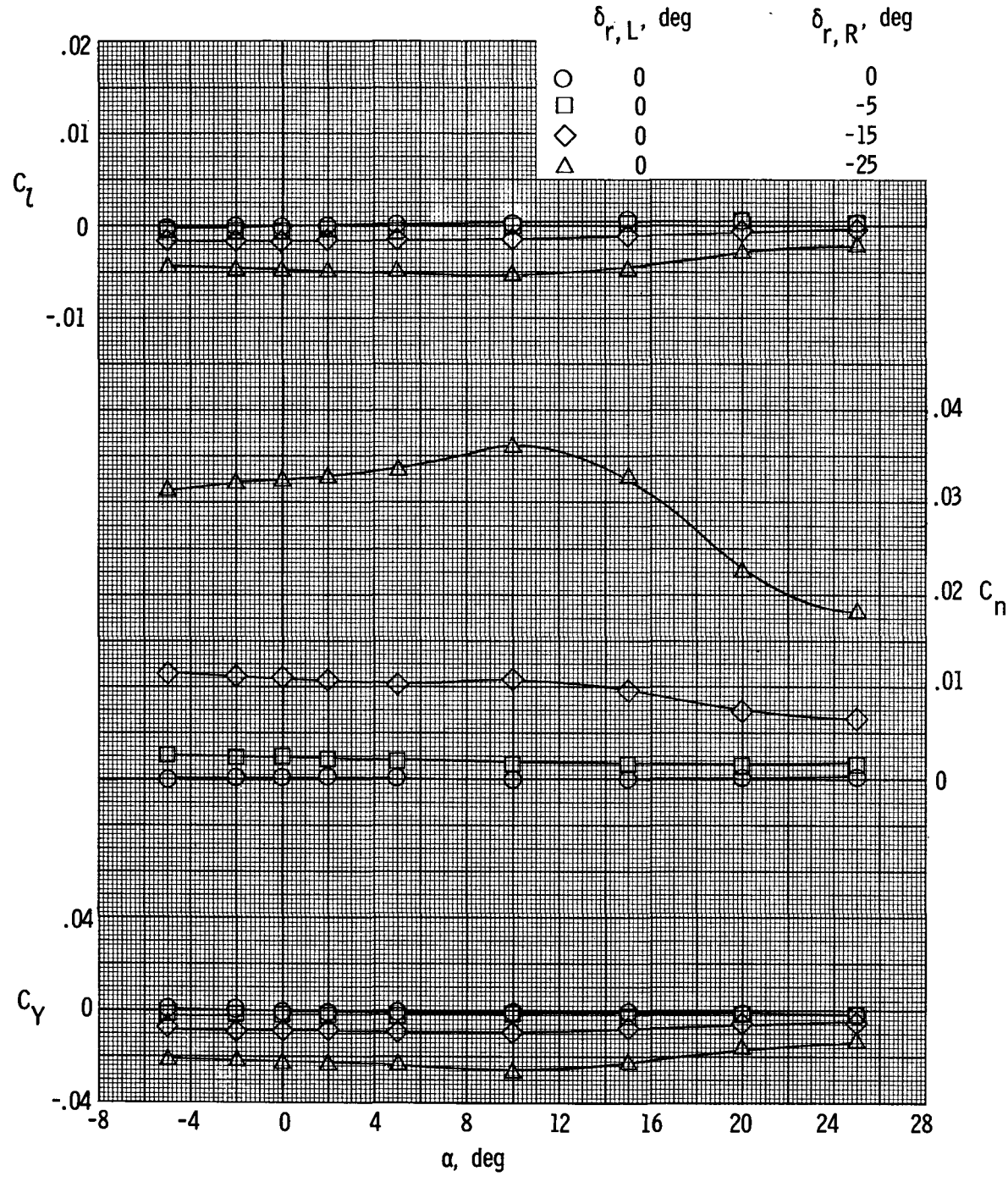

(a) Yaw control data.

Figure 11.- Effects of rudder deflection on yaw control, performance, and stability characteristics of configuration BW_2E_2F. $\delta_n = 5^o$; $\delta_e = 0^o$; M = 9.6.

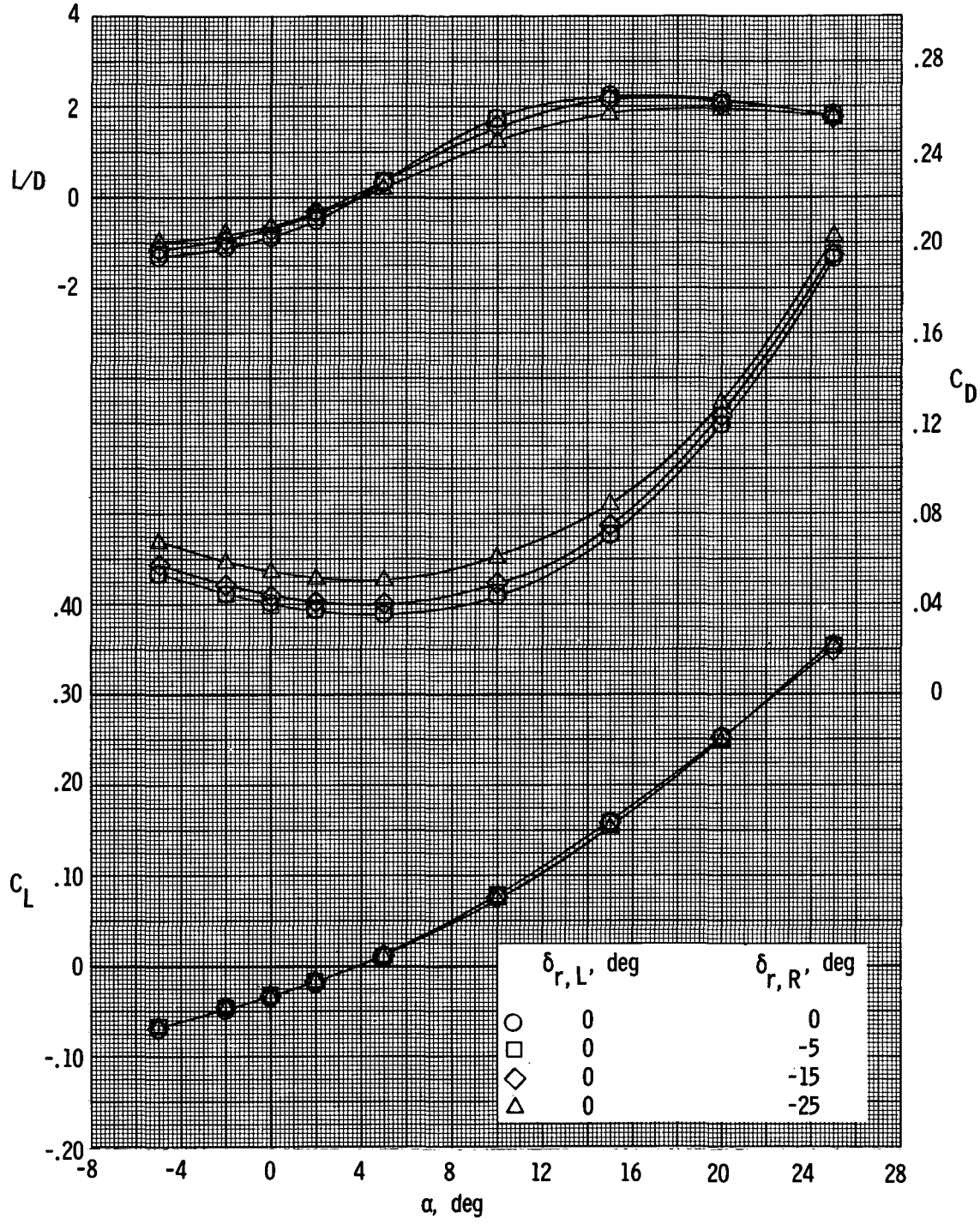

(b) Performance data.

Figure 11.- Continued.

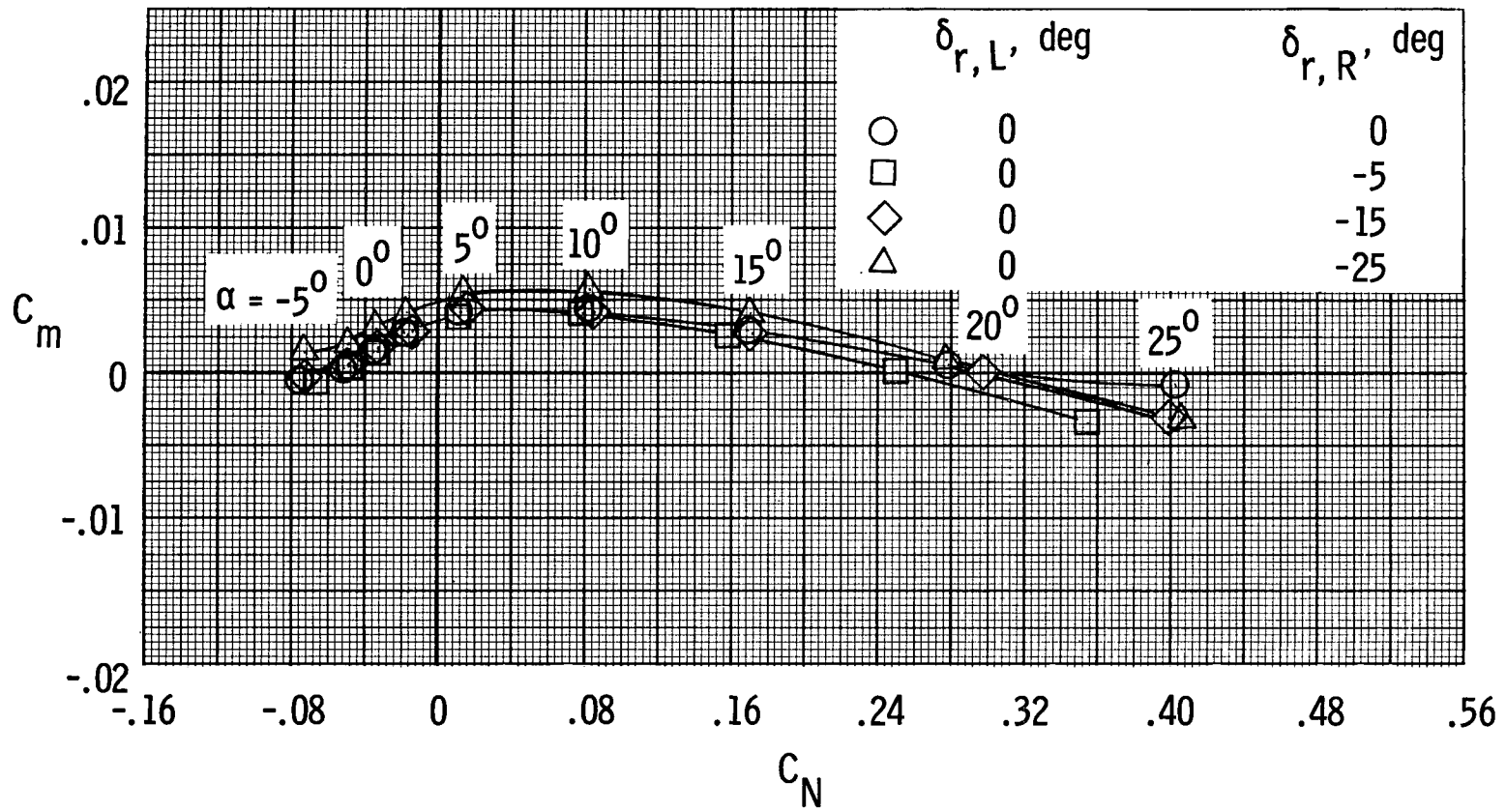

(c) Stability data.

Figure 11.- Concluded.

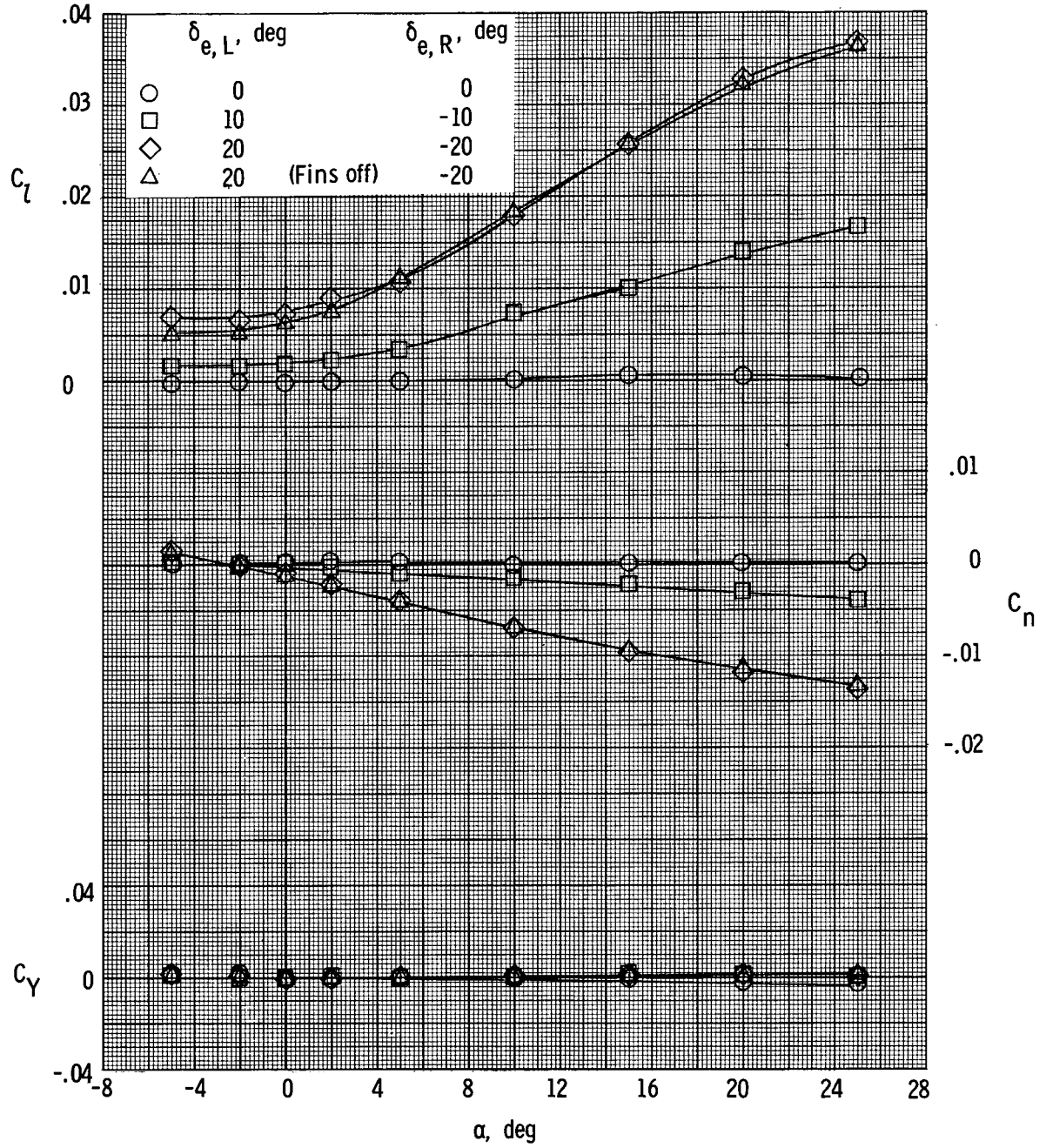

(a) Roll control data.

Figure 12.- Effects of differential elevon deflection on roll control, performance, and stability characteristics of configuration BW_2E_2F. $\delta_n = 5^o$; $\delta_r = 0^o$; M = 9.6.

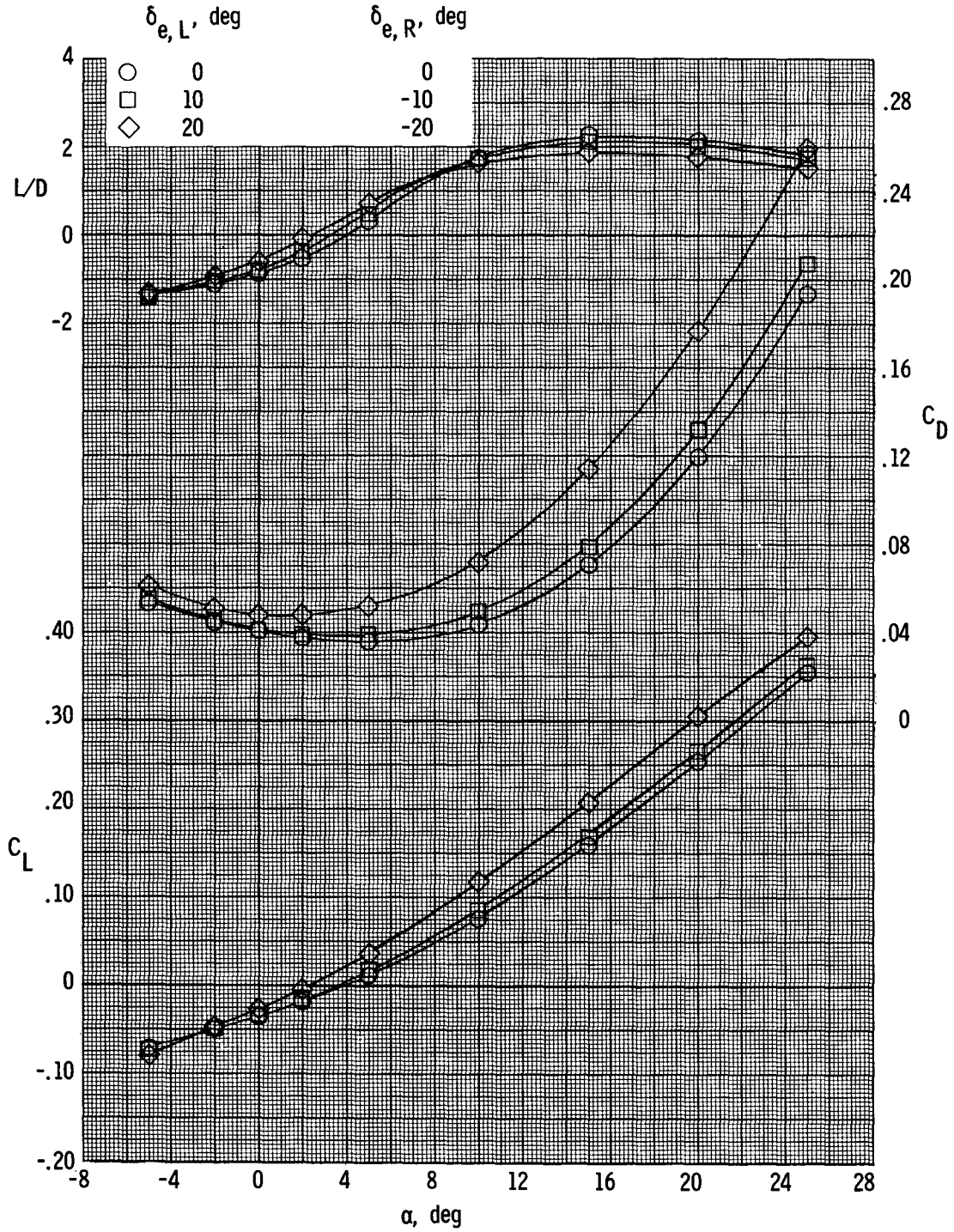

(b) Performance data.

Figure 12.- Continued.

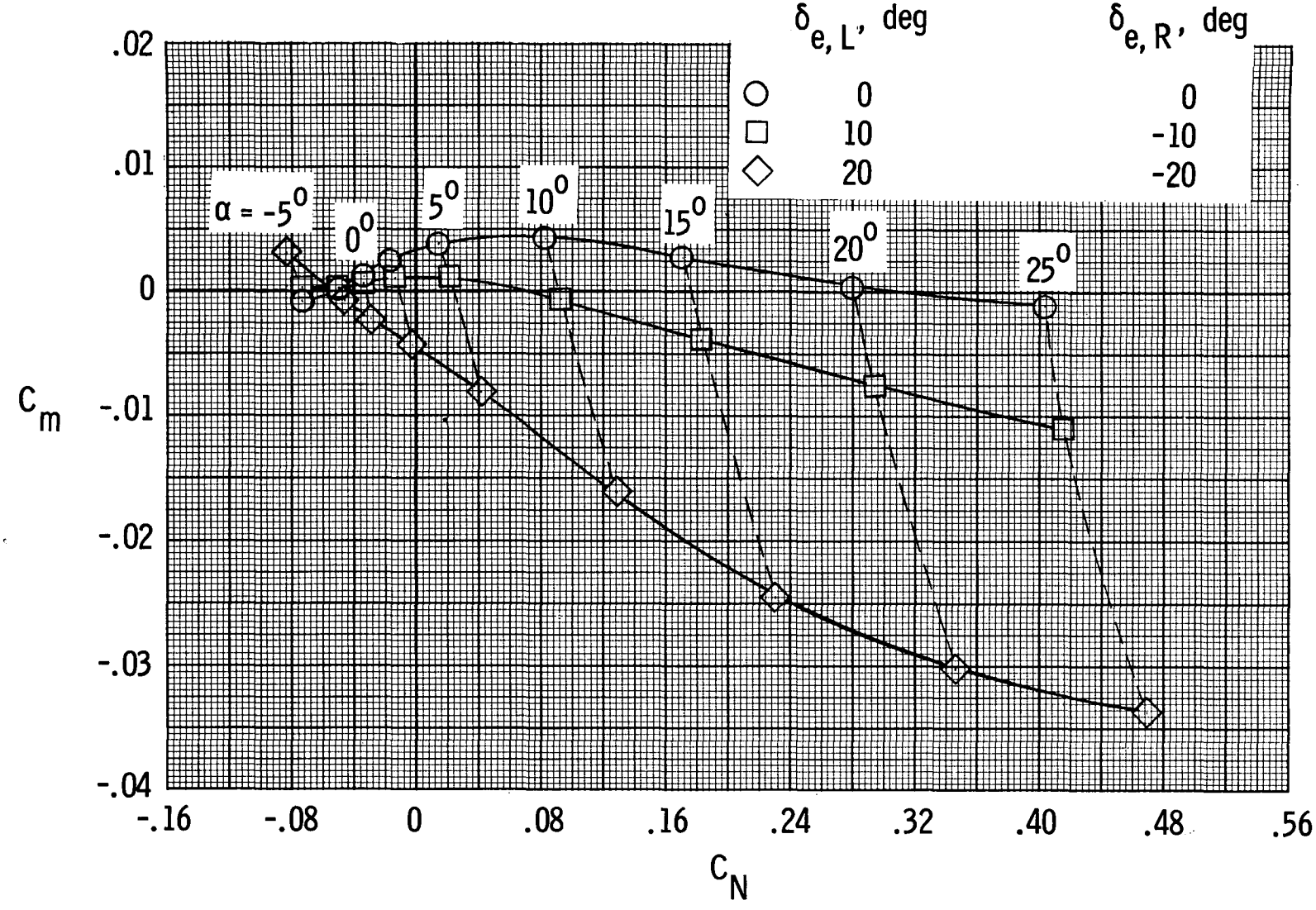

(c) Stability data.

Figure 12.- Concluded.

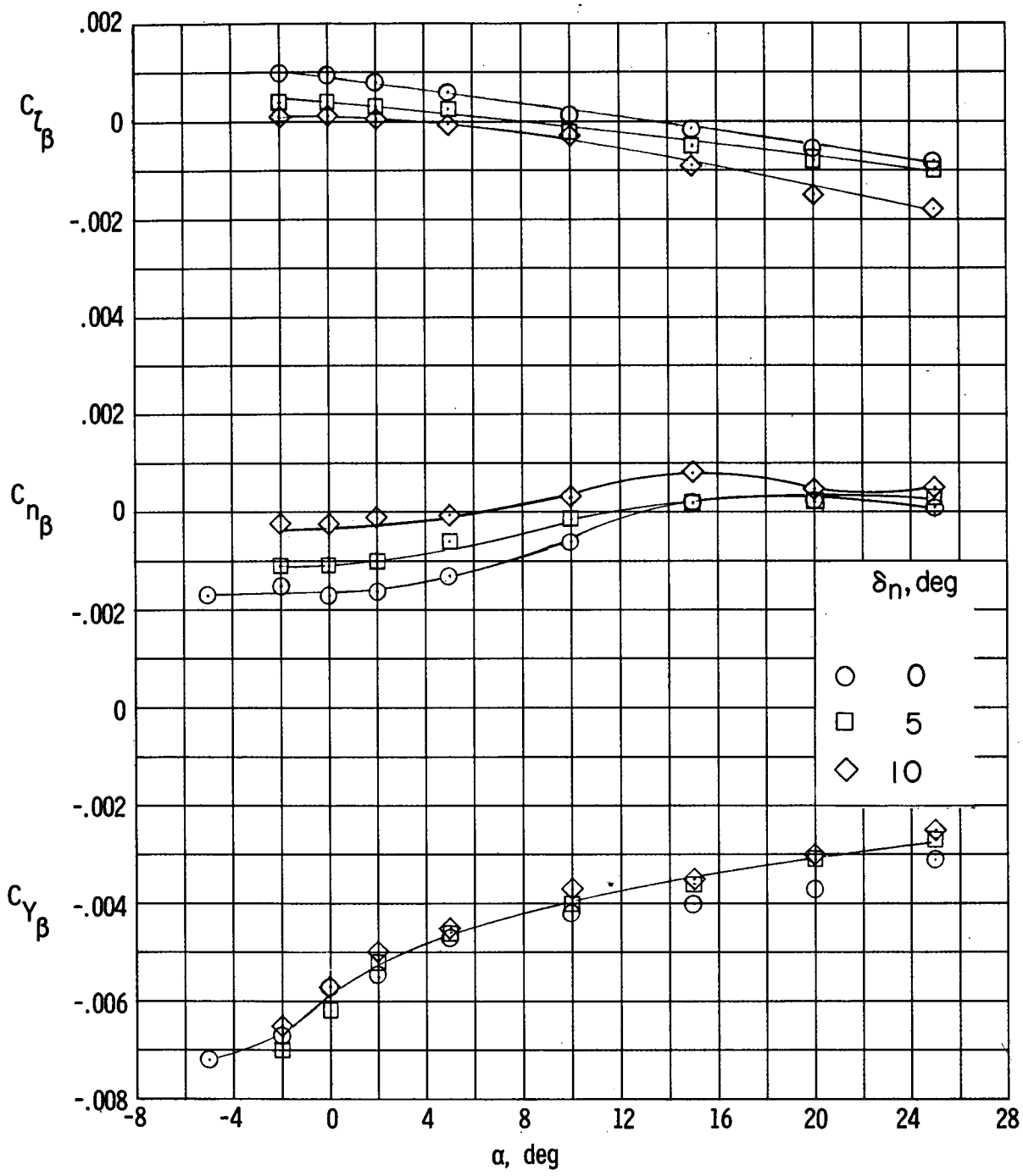

Figure 13.- Effects of nose deflection angle on the directional and lateral stability characteristics of configuration BW_2E_2F. $\delta_r = 0^\circ$; $\delta_e = 0^\circ$; M = 9.6.

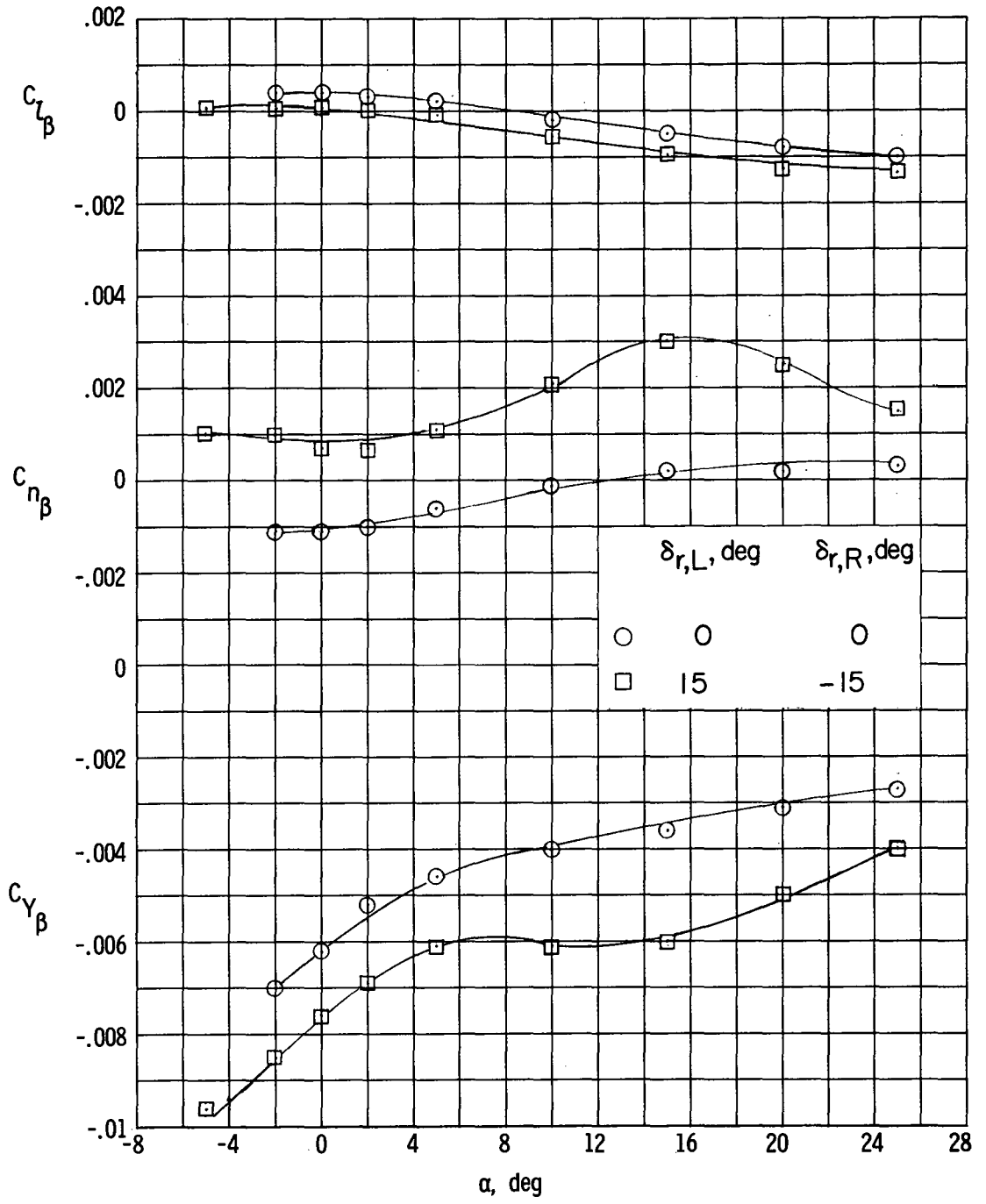

(a) Directional and lateral stability data.

Figure 14.- Effects of deflecting both rudders outboard on the directional and lateral stability and the longitudinal stability and performance characteristics of configuration BW_2E_2F. $\delta_n = 5^o$; $\delta_e = 0^o$; M = 9.6.

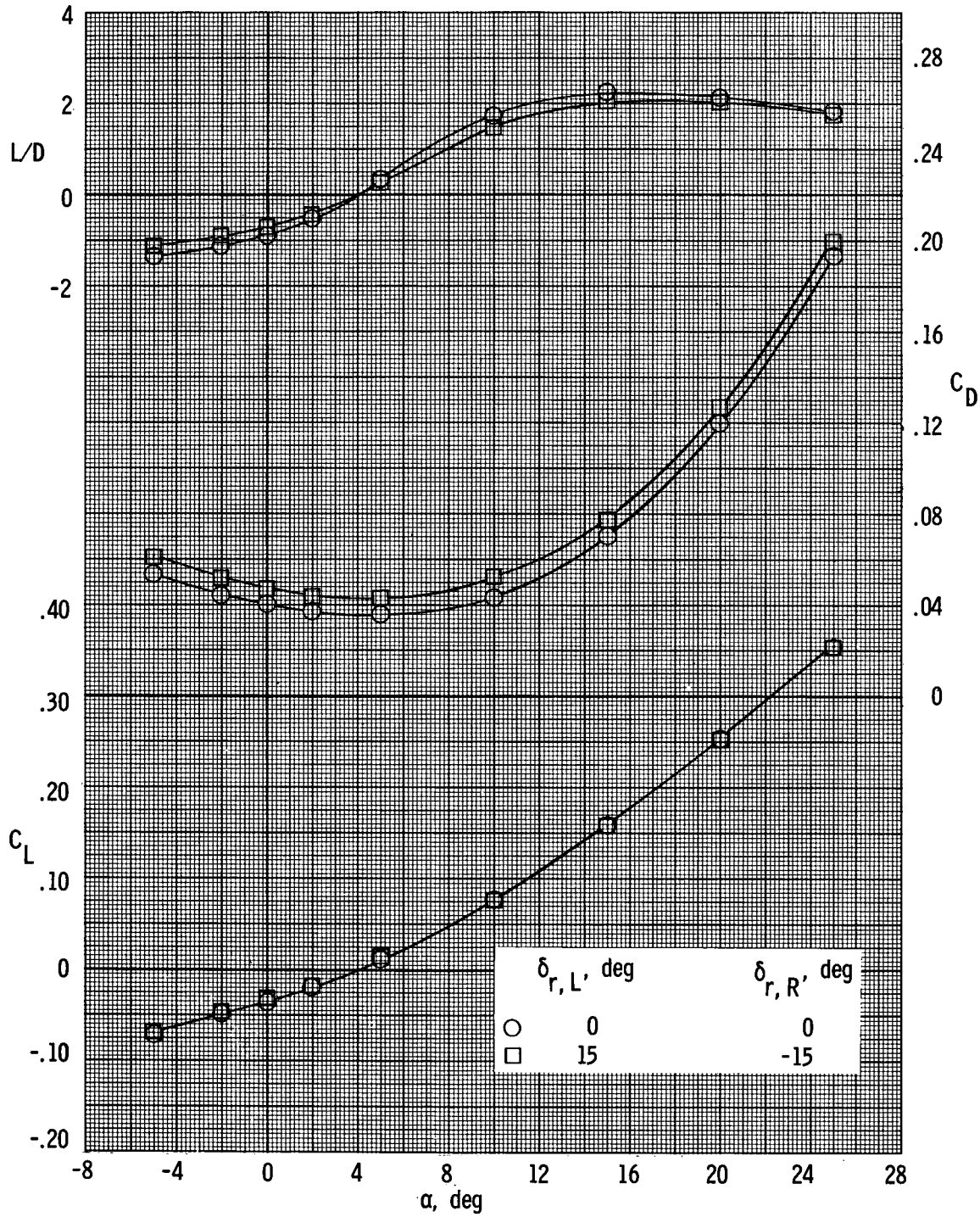

(b) Longitudinal performance data.

Figure 14.- Continued.

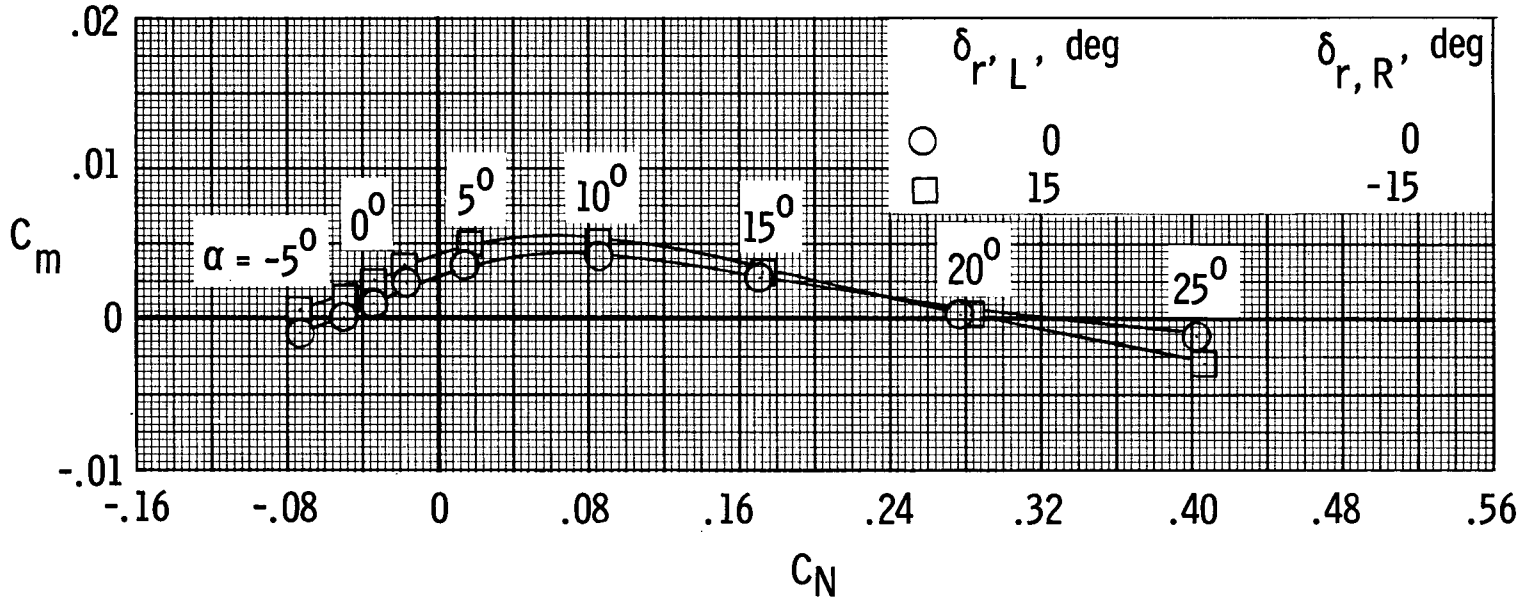

(c) Stability data.

Figure 14.- Concluded.

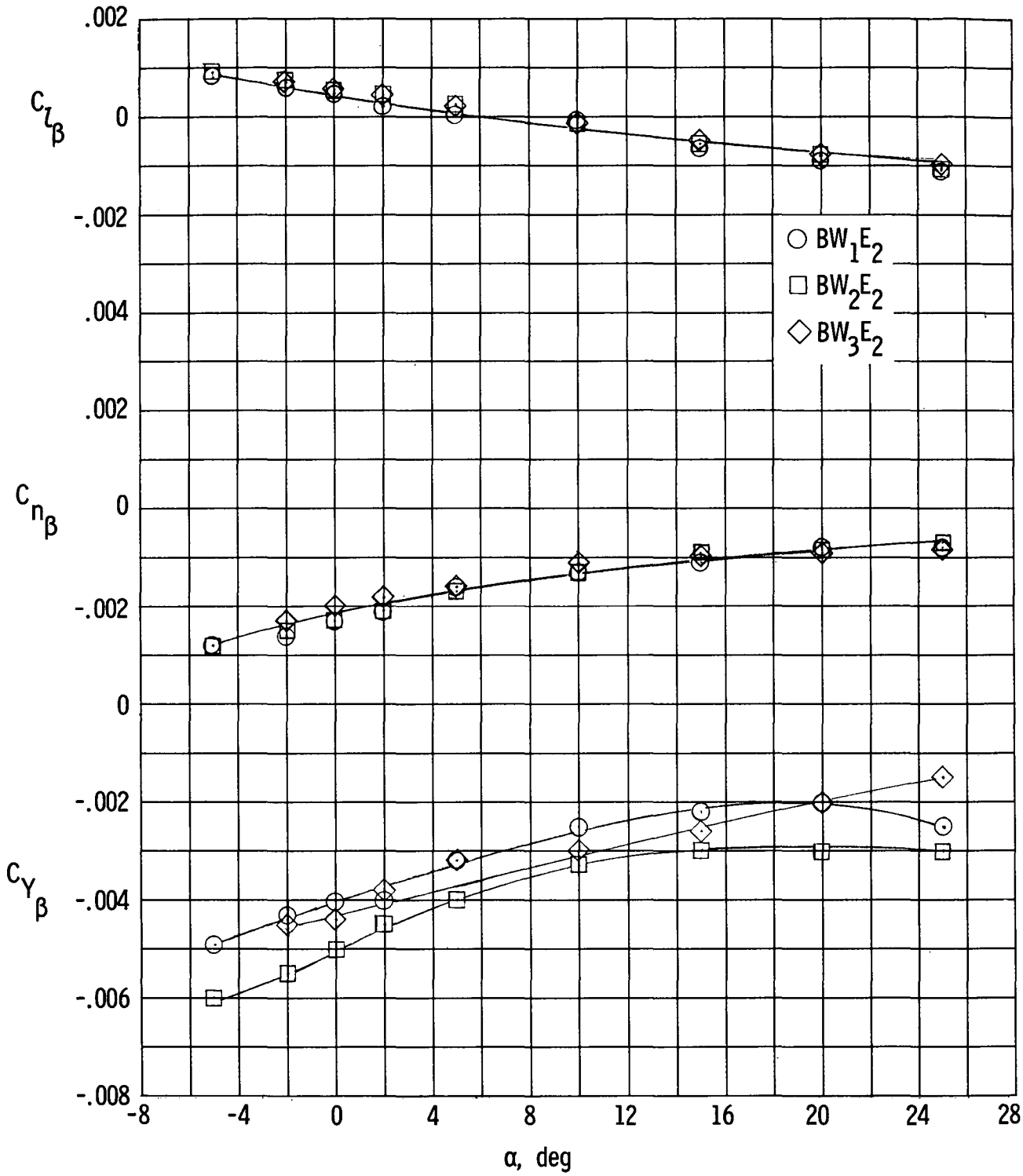

Figure 15.- Effects of wing section on the directional and lateral stability characteristics. $\delta_n = 5^\circ$; $\delta_r = 0^\circ$; $\delta_e = 0^\circ$; M = 9.6.

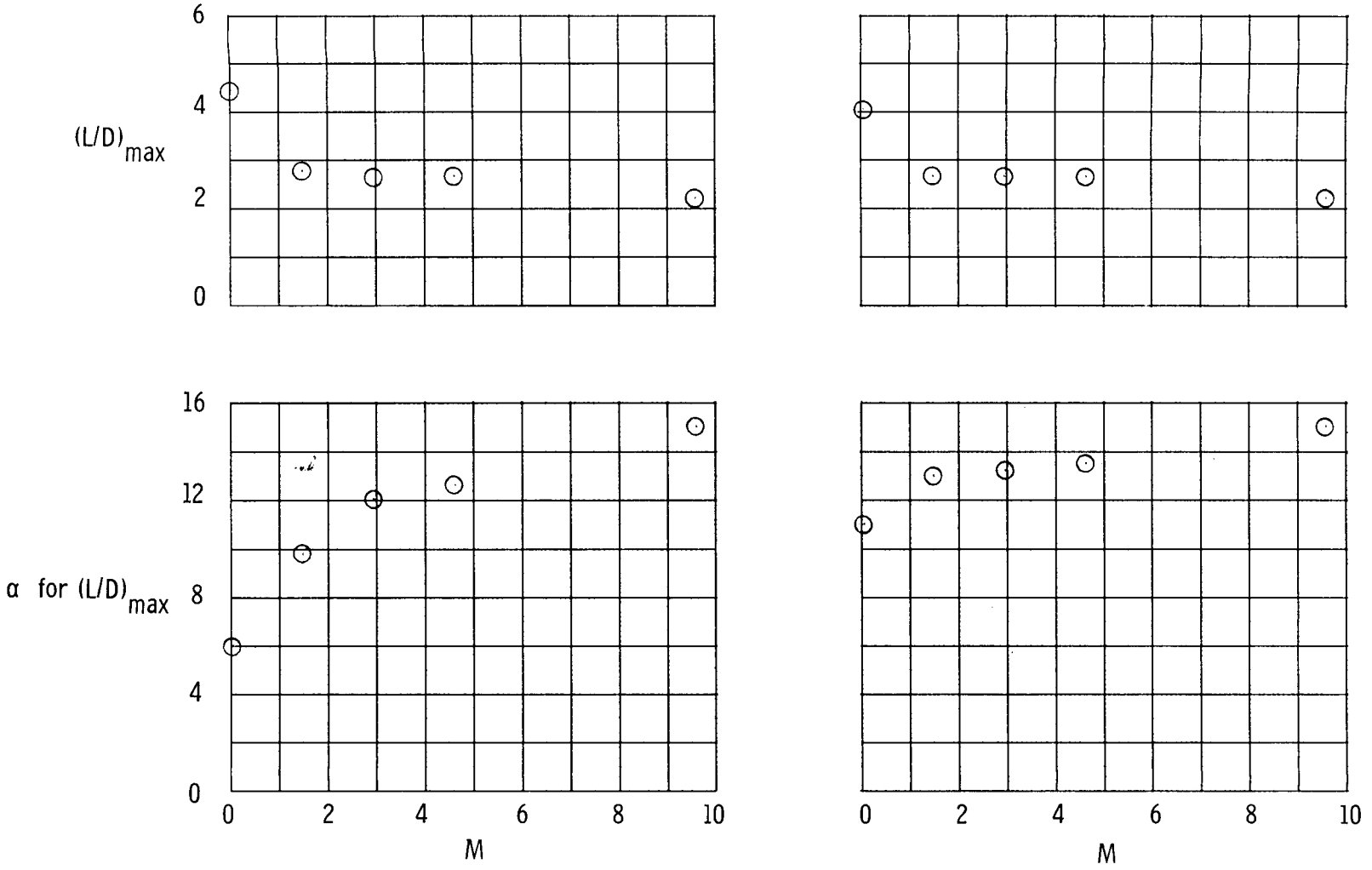

(a) $\delta_e = 0°$.

(b) $\delta_e = -10°$.

Figure 16. Effects of Mach number on the performance characteristics of configuration BW_2E_1F. $\delta_n = 5°$; $\delta_r = 0°$.

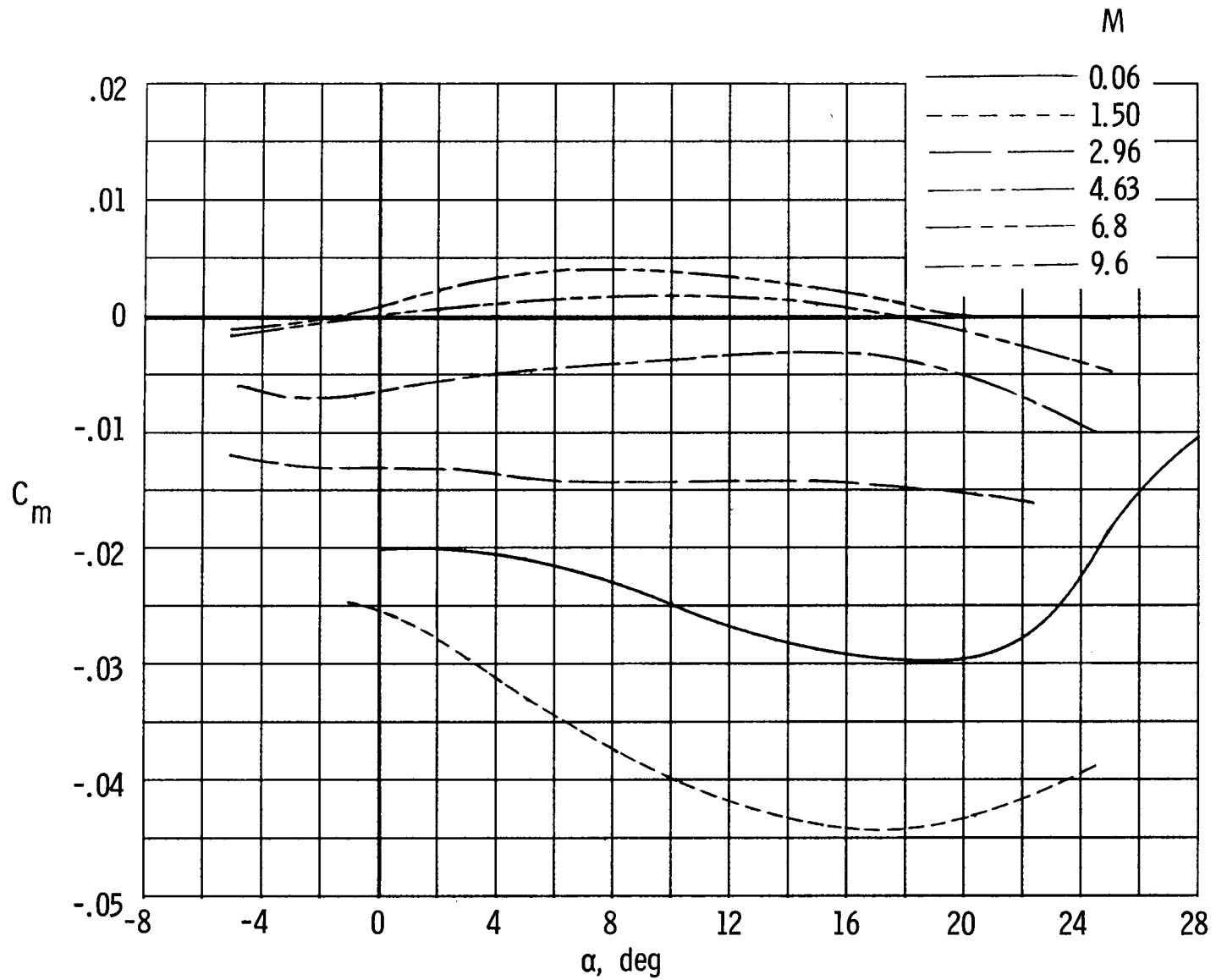

(a) $\delta_e = 0^\circ$.

Figure 17.- Effects of Mach number on the longitudinal stability characteristics of configuration BW_2E_1F. $\delta_n = 5^\circ$; $\delta_r = 0^\circ$.

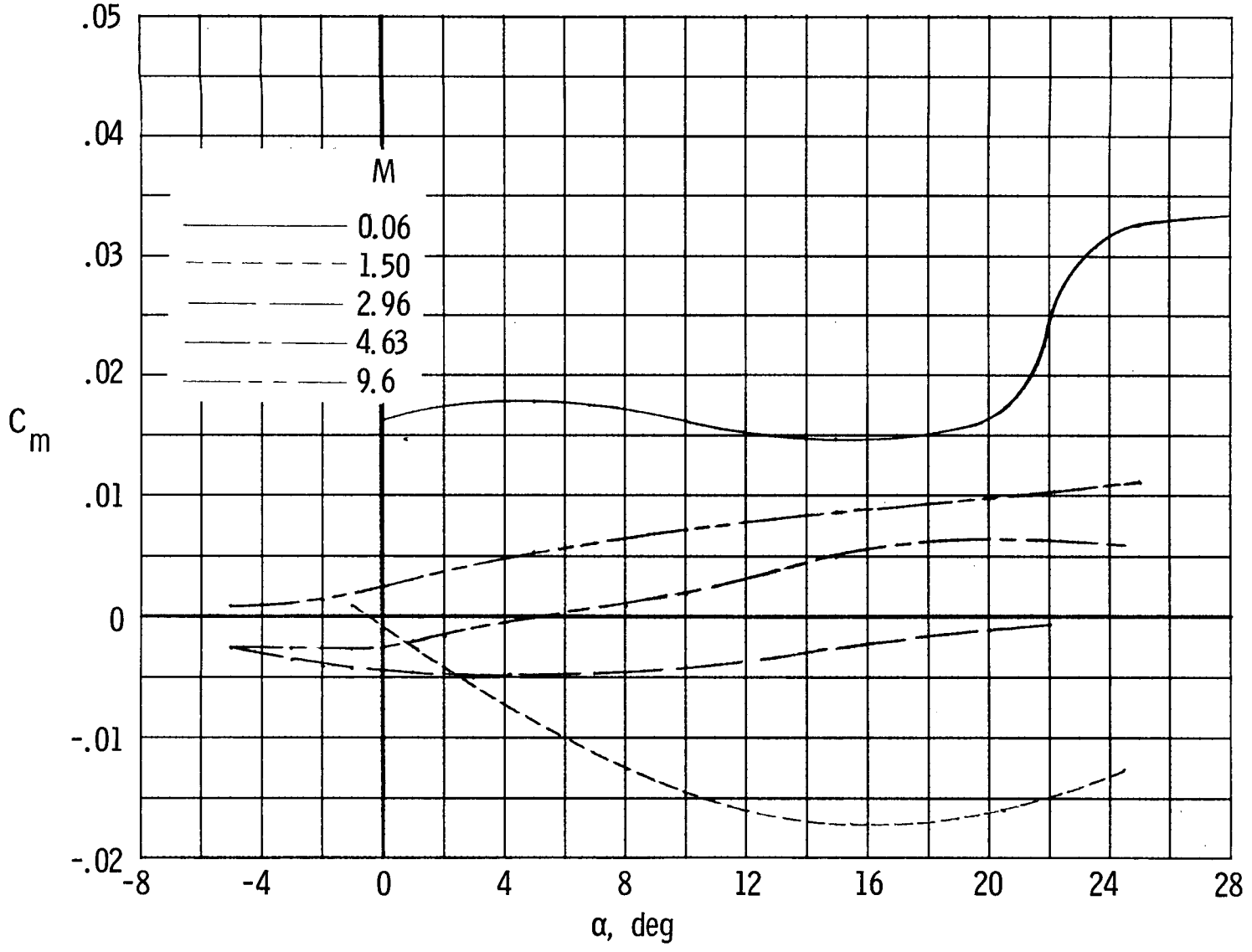

(b) $\delta_e = -10^\circ$.

Figure 17.- Continued.

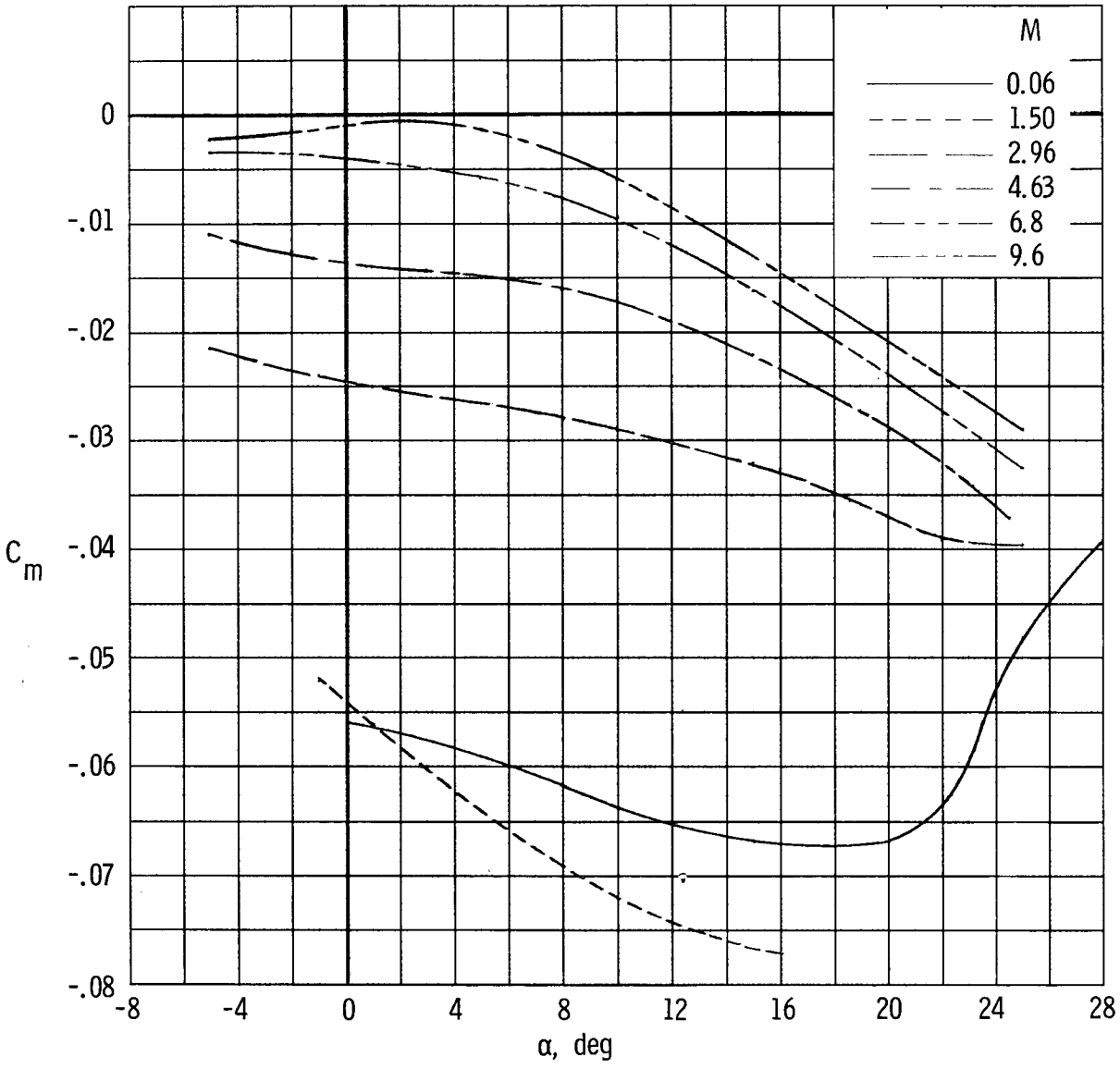

(c) $\delta_e = 10^\circ$.

Figure 17.- Concluded.

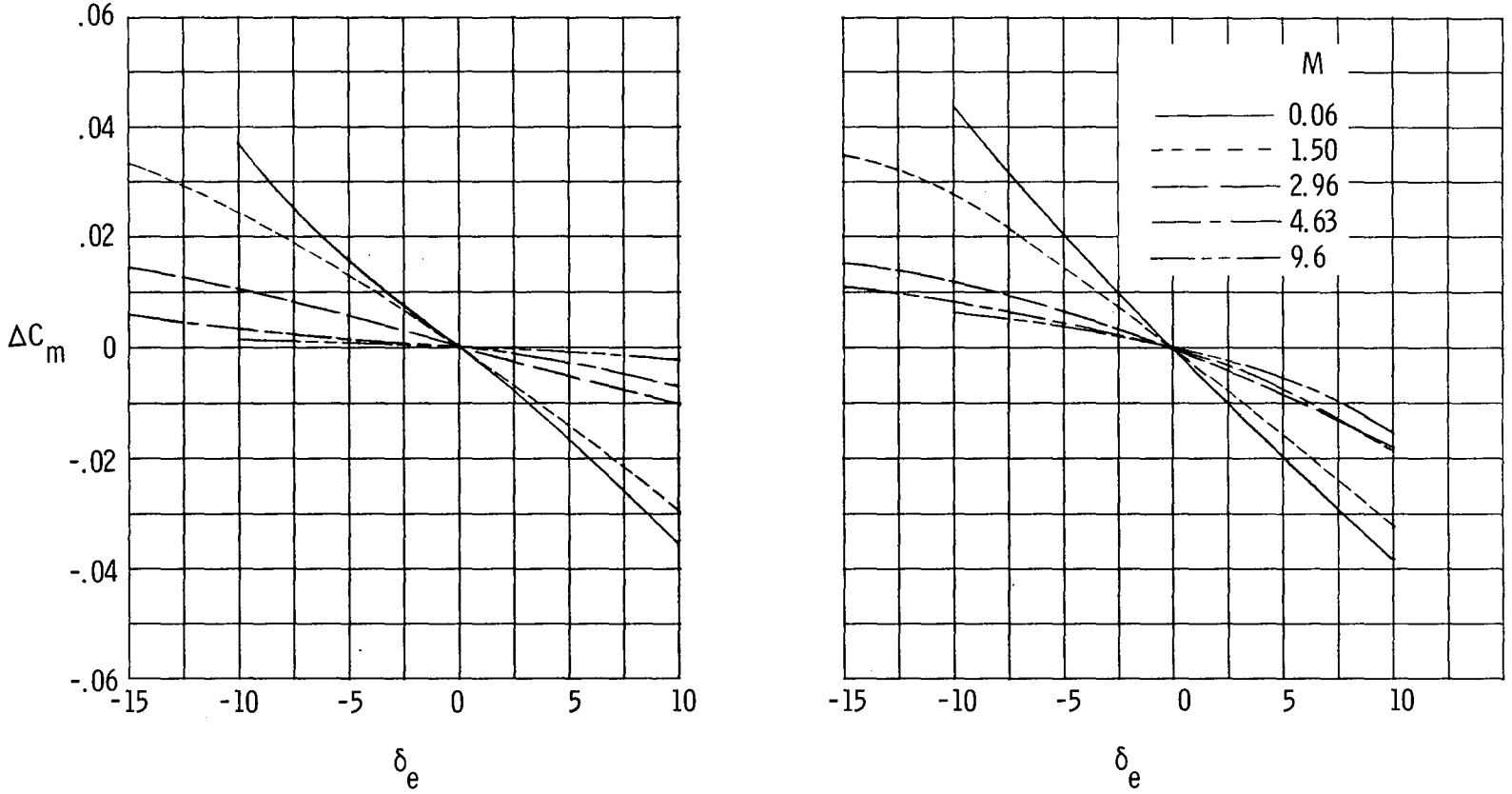

(a) $\alpha = 0^\circ$.

(b) $\alpha = 15^\circ$.

Figure 18.- Effects of Mach number on the incremental pitching moments of configuration BW_2E_1F. $\delta_n = 5^\circ$; $\delta_r = 0^\circ$.

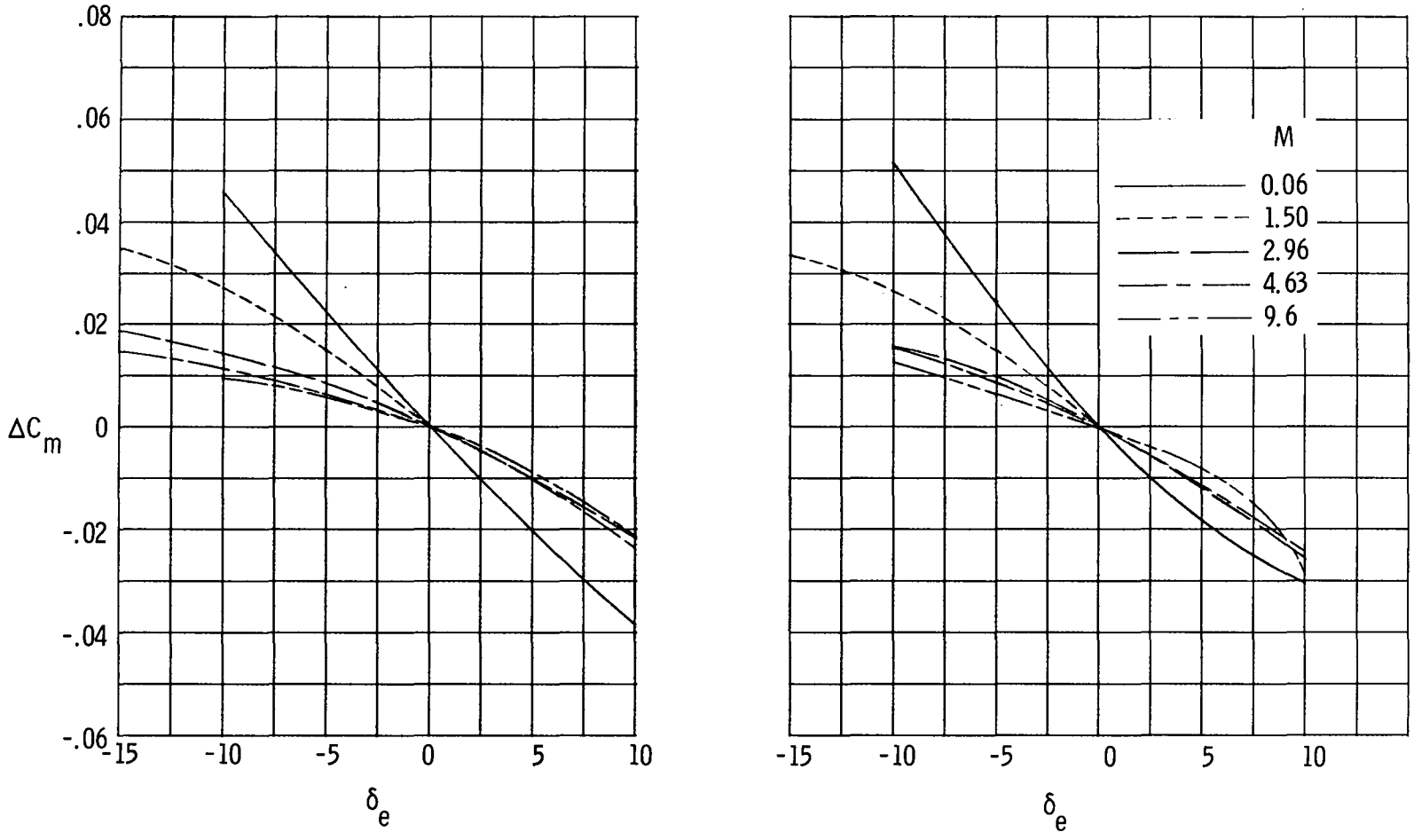

(c) $\alpha = 20°$.

(d) $\alpha = 25°$.

Figure 18.- Concluded.

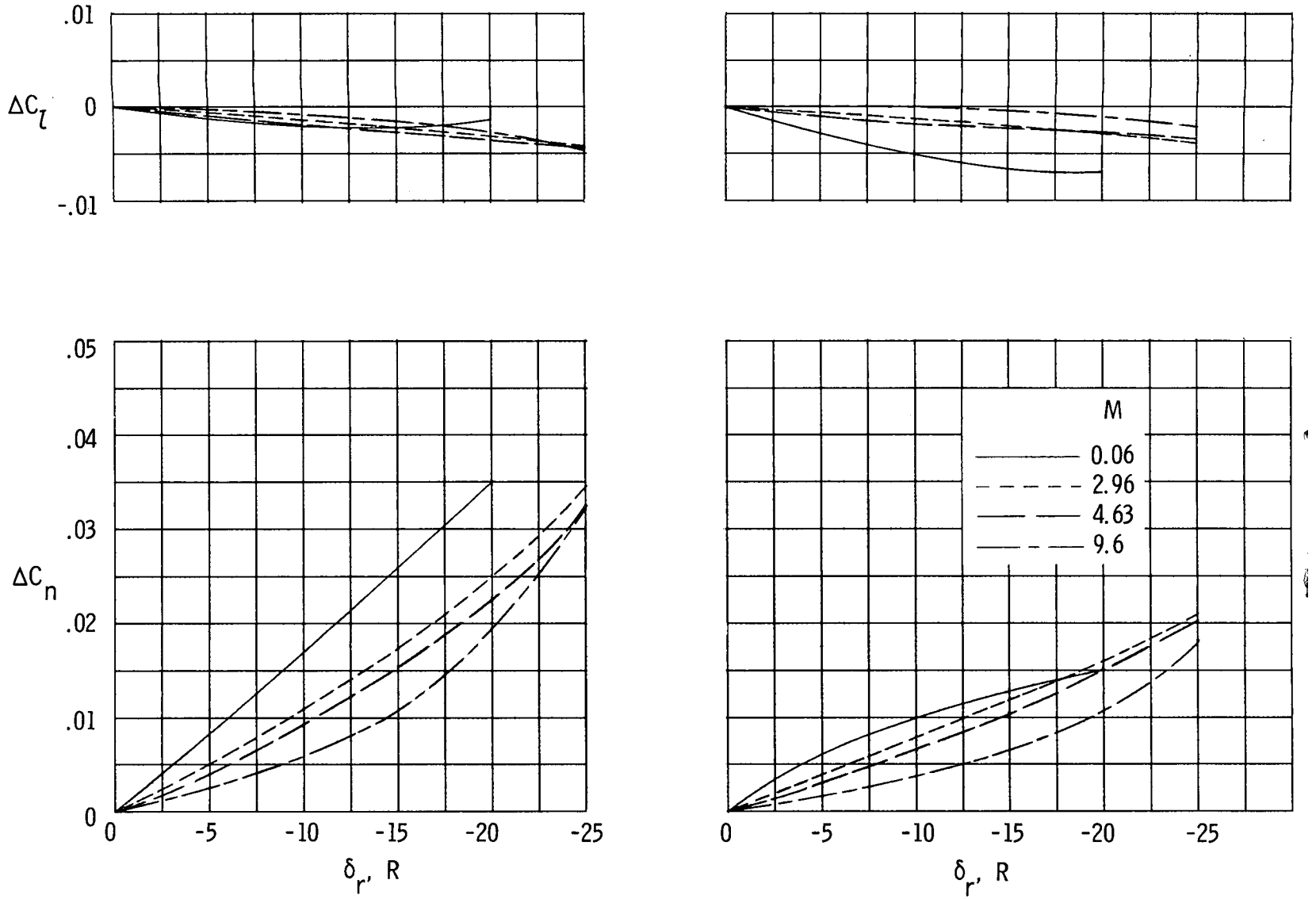

(a) $\alpha = 0^\circ$.

(b) $\alpha = 25^\circ$.

Figure 19.- Effects of Mach number on the yaw control characteristics of configuration BW_2E_1F. $\delta_n = 0^\circ$; $\delta_e = 0^\circ$.

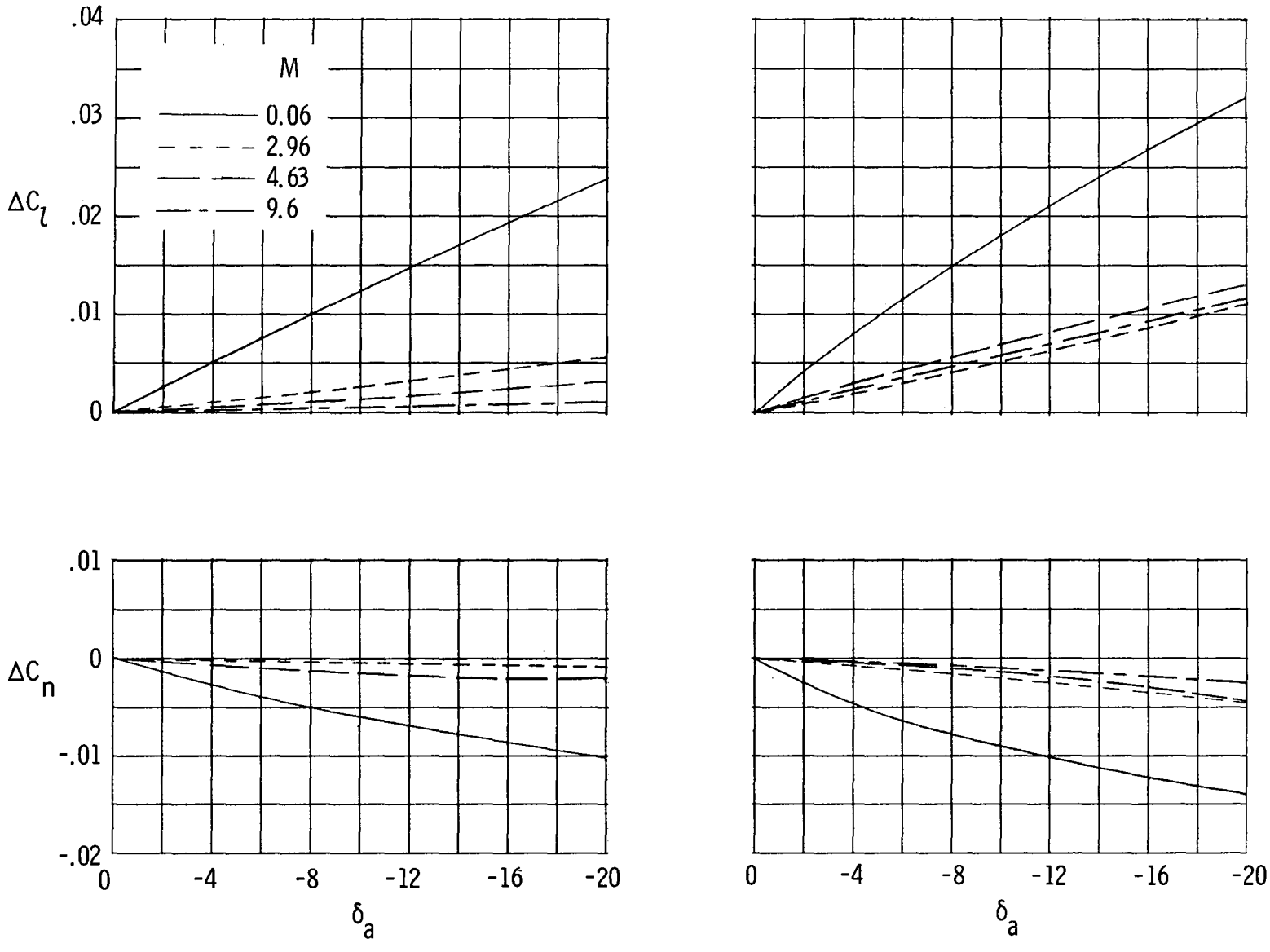

(a) $\alpha = 0^\circ$.

(b) $\alpha = 25^\circ$.

Figure 20.- Effects of Mach number on the roll control characteristics of configuration BW_2E_1F. $\delta_n = 5^\circ$; $\delta_r = 0^\circ$.

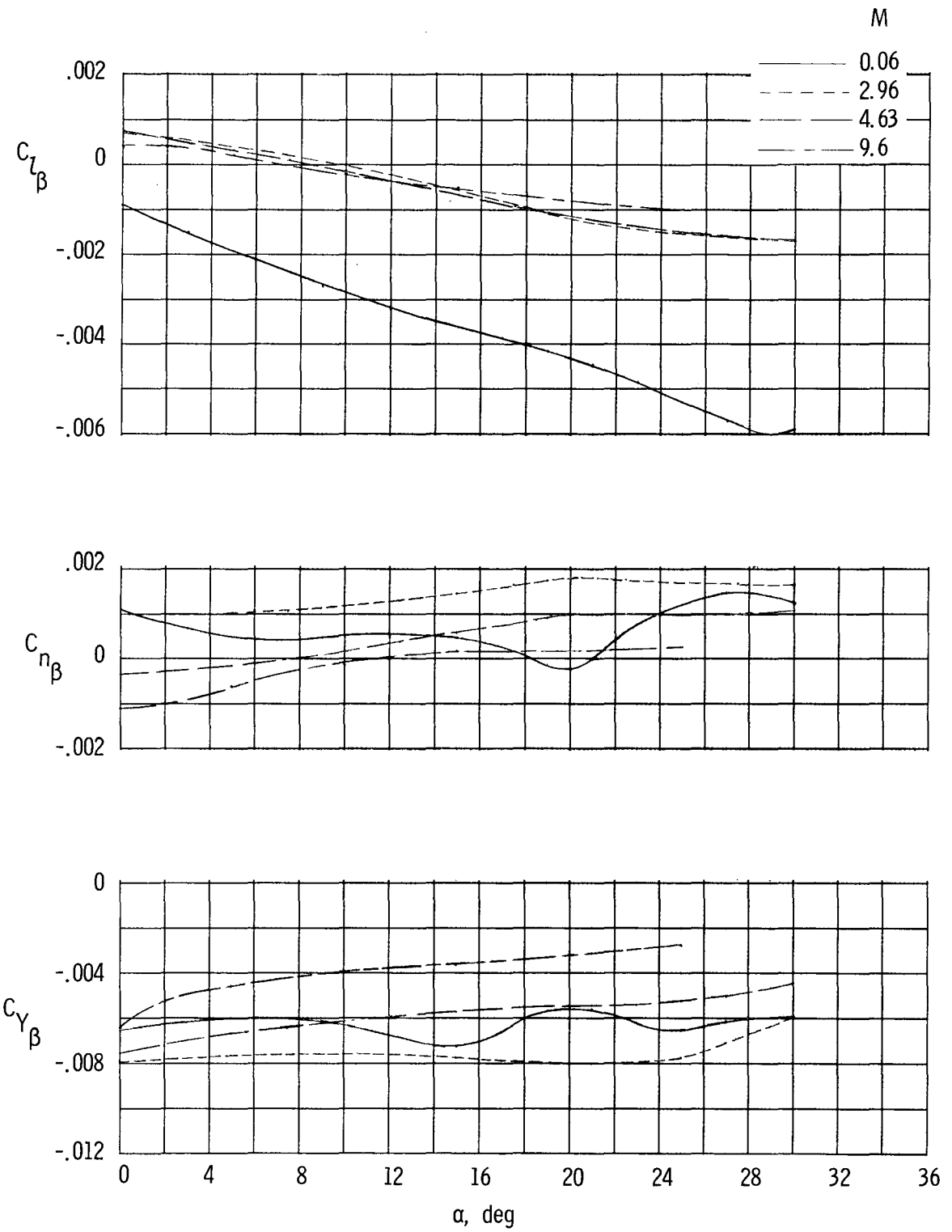

Figure 21.- Effects of Mach number on the directional and lateral stability characteristics of configuration BW_2E_1F. $\delta_n = 5^\circ$; $\delta_e = 0^\circ$; $\delta_r = 0^\circ$.